

# 1 Anticipating regime shifts by mixing early warning 2 signals from different nodes

3 Naoki Masuda<sup>a,b,\*</sup>, Kazuyuki Aihara<sup>c</sup>, and Neil G. MacLaren<sup>a</sup>

4 <sup>a</sup>Department of Mathematics, State University of New York at Buffalo, Buffalo, NY, 14260-2900, USA

5 <sup>b</sup>Institute for Artificial Intelligence and Data Science, State University of New York at Buffalo, Buffalo, NY,  
6 14260-5030, USA

7 <sup>c</sup>International Research Center for Neurointelligence, The University of Tokyo Institutes for Advanced Study, The  
8 University of Tokyo, Japan

9 \*naokimas@gmail.com

## 10 ABSTRACT

11 Real systems showing regime shifts, such as ecosystems, are often composed of many dynamical elements interacting on  
a network. Various early warning signals have been proposed for anticipating regime shifts from observed data. However,  
it is unclear how one should combine early warning signals from different nodes for better performance. Based on theory  
of stochastic differential equations, we propose a method to optimize the node set from which to construct an early warning  
signal. The proposed method takes into account that uncertainty as well as the magnitude of the signal affects its predictive  
performance, that a large magnitude or small uncertainty of the signal in one situation does not imply the signal's high  
performance, and that combining early warning signals from different nodes is often but not always beneficial. The method  
performs well particularly when different nodes are subjected to different amounts of dynamical noise and stress.

## 12 Introduction

13 Real complex systems often experience sudden and substantial changes, also referred to as regime shifts or tipping events,  
14 as environments or the system's internal properties gradually change. Such sudden changes often alter functions of the  
15 system, sometimes in an irreversible manner. Tipping phenomena have been used to explain, for example, mass extinctions in  
16 ecosystems<sup>1,2</sup>, deforestation<sup>3,4</sup>, onset of epidemic spreading<sup>5</sup>, and progression of mental disorders<sup>6-8</sup> and other diseases<sup>9,10</sup>. No  
17 matter whether the system transits from a desirable state to an undesirable one (e.g., species' extinctions, epidemic spreading)  
18 or vice versa (e.g., recovery from disease), one is generally interested in anticipating a large regime shift due to a tipping event  
19 before it occurs. From dynamical systems points of view, a tipping event probably most famously corresponds to a change in  
20 the stability of an equilibrium. Theory suggests that critical slowing down happens near such a tipping point, which one can  
21 exploit to construct early warning signals for an impending tipping event<sup>1,11</sup>. Various early warning signals for tipping events,  
22 which can be applied to observed data without knowledge of the dynamical system equations, have been proposed<sup>1,5,10-15</sup>.

23 Complex systems whose tipping points we want to anticipate are more often than not composed of dynamical elements  
24 interacting on a network. In an ecosystem, animals, plants, or microbial species, for example, are interconnected by mutualistic,  
25 prey-predator, and other types of interactions. In a climate system, geographical regions are interconnected by, for example,  
26 water and heat transport. Network resilience is a comprehensive approach with which to understand how dynamics on networks  
27 respond to perturbations and system failures<sup>16</sup>. For dynamics on networks that possibly show tipping events and are relevant to  
28 these applications, it is highly likely that the network structure is complex<sup>17,18</sup> and that, related to this, all the nodes do not emit  
29 equally useful early warning signals<sup>19-24</sup>. Specifically, nodes that are about to tip may be emitting more useful early warning  
30 signals than other nodes in the same system that are still far from tipping. Evidence in favor of this view is that, as a dynamical  
31 system gradually changes, some nodes may tip earlier than others, showing multistage transitions<sup>11,25-29</sup>. Therefore, selecting  
32 an appropriate set of sentinel nodes from which one calculates the early warning signal may improve the quality of the signal in  
33 addition to saving the cost of observing uninformative nodes.

34 Several methods for selecting a sentinel node set, denoted by  $S$ , for constructing early warning signals have been proposed.  
35 The dynamical network biomarker theory searches for an  $S$  that maximizes a composite index<sup>9,10,30,31</sup>. The index is the average  
36 pairwise correlation of the sample of data between the nodes within  $S$  multiplied by the standard deviation of the samples across  
37 the nodes in  $S$ , which is divided by the average pairwise correlation of the samples between a node in  $S$  and a node outside  
38  $S$ . Another analytical approach is to identify a multidimensional linear dynamics model near the bifurcation point only from  
39 observed data and then use the dominant eigenvector associated with the estimated dynamics to select  $S$  (i.e., as the set of

40 the  $i$ th nodes such that the  $i$ th entry of the dominant eigenvector is the largest in terms of the absolute value<sup>23</sup>. Note that an  
 41 earlier study pointed out the usefulness of the dominant eigenvector<sup>19</sup>. Participation of the node in the dominant eigenvector is  
 42 also used for selecting  $S$  in other studies<sup>21,24</sup>. In addition, an eigenvector-based method has also been proposed for ranking  
 43 the nodes most sensitive to perturbations<sup>32</sup>. A different study numerically showed that nodes with small degrees (i.e., small  
 44 number of the neighboring nodes) are good performers<sup>20</sup>. A method to determine  $S$  based on network control theory also found  
 45 an advantage of selecting nodes with small degrees<sup>27</sup>. Using the nodes receiving the highest total input from other nodes is  
 46 also a powerful heuristic for setting  $S$ <sup>29</sup>. Simply using the nodes with the highest fluctuations also improves upon other naive  
 47 methods<sup>29</sup>. Note that the last two methods are often better than using all the nodes in the network as  $S$ , and the same may be  
 48 true for other node selection methods.

49 Except for the dynamical network biomarker theory, these methods provide ranking of nodes and suggest that we should  
 50 include the top-ranked nodes in  $S$ . It is unclear whether combining the nodes in  $S$  improves an early warning signal compared  
 51 to when the single top node in  $S$  is used. Any early warning signal (e.g., variance of the signal, lagged autocorrelation) is  
 52 noisy because, by design, an early warning signal exploits the information about impending tipping events hidden in noisy  
 53 observations. If a given early warning signal measured for each  $i$ th node is independent for the different nodes in  $S$ , then  
 54 averaging them including the case of a weighted average is expected to produce a better early warning signal owing to the  
 55 central limit theorem. Quantitatively, the standard deviation of the early warning signal should decrease according to  $\propto n^{-1/2}$ ,  
 56 where  $n$  is the number of nodes in  $S$ , and  $\propto$  represents “in proportion to”. However, nodes in a complex system are interrelated,  
 57 such as through edges in the case of conventional networks, and the states of different nodes are correlated in general<sup>33-35</sup>.  
 58 Therefore, it is not a trivial concern whether or not combination of the top-ranked nodes generates a high-quality early warning  
 59 signal. For example, suppose that  $S$  is composed of  $n$  nodes close to each other in the network and that the states of these  $n$   
 60 nodes are hence strongly correlated. In this case, averaging the early warning signals over the  $n$  nodes does not help much to  
 61 reduce their fluctuation because the  $n$  early warning signals are similar to each other. We may be then tempted to select  $n$  nodes  
 62 that are far from each other on the network even if some of the  $n$  nodes do not provide early warning signals of top quality.

63 In fact, the aforementioned dynamical network biomarker theory aims to optimize the set  $S$ , which the original authors call  
 64 the dominant group, implicitly resolving this problem<sup>9,10,30,31</sup>. However, the composite index that they propose is heuristic,  
 65 and why this method works well in medical applications<sup>10,36</sup> and how the effectiveness of their method translates to other  
 66 applications such as in ecology are elusive. Furthermore, this theory and most other proposals of early warning signals neglect  
 67 that early warning signals are themselves noisy. Considering fluctuations of early warning signals in their design is necessary  
 68 for at least two reasons. First, if a candidate early warning signal carries a lot of noise, then that signal may not be useful even  
 69 if its expected value is sensitive to the approach of the system towards the tipping point. A recent study highlighted interplay  
 70 of the dominant eigenvector direction of the Jacobian matrix of the dynamics and the primary noise direction that is dragged  
 71 towards the nodes receiving high dynamical noise<sup>24</sup>. Second, in the aforementioned example of  $n$  nodes, let us assume that  
 72 the expectation of the single-node early warning signal is the same for all the  $n$  nodes. We stated that averaging over the  $n$   
 73 early warning signals would be beneficial relative to the single-node early warning signals only if the  $n$  signals are not strongly  
 74 correlated with each other. In this situation, the expectation of the averaged early warning signal is the same as that of the  
 75 single-node early warning signal. The bonus of the averaging is only present in the reduced fluctuation in the averaged as  
 76 opposed to the single-node early warning signal. To enable such discussion, we need to assess the fluctuation as well as the  
 77 magnitude of early warning signals.

78 In the present study, we develop a mathematical framework for node set selection for early warning signals based on  
 79 stochastic differential equations on networks. By assuming dynamics near the equilibrium and using the variance of the node’s  
 80 state as the early warning signal, we propose an index whose maximization gives an optimal node set for constructing an early  
 81 warning signal. We demonstrate our method with analytically solvable networks with two or three nodes and with numerically  
 82 investigated larger networks combined with various dynamics models.

## 83 Results

### 84 Theory

We consider an  $N$ -dimensional noisy nonlinear dynamical system in continuous time. We regard each of the  $N$  dynamical  
 elements as a node and the entire dynamical system as stochastic dynamics on a network with  $N$  nodes. We denote by  $x_i(t) \in \mathbb{R}$   
 the state of the  $i$ th node at time  $t \in \mathbb{R}$ . We write  $\mathbf{x}(t) = (x_1(t), \dots, x_N(t))^\top$ , where  $^\top$  represents the transposition. We assume  
 that  $\mathbf{x}(t)$  obeys a set of stochastic differential equations in the Itô sense given by

$$85 \quad d\mathbf{x}(t) = F(\mathbf{x}(t))dt + B dW(t), \quad (1)$$

86 where  $F : \mathbb{R}^N \rightarrow \mathbb{R}^N$ ;  $B$  is an  $N \times N$  matrix;  $W(t)$  represents a  $N$ -dimensional vector of independent Wiener processes (i.e.,  
 white noise).

Assume that the dynamics given by Eq. (1) has an equilibrium in the absence of noise, which we denoted by  $\mathbf{x}^* = (x_1^*, \dots, x_n^*)^\top$ . By linearizing Eq. (1) around  $\mathbf{x}^*$ , we obtain a set of linear stochastic differential equations given by

$$d\mathbf{z}(t) = -A\mathbf{z}(t)dt + BdW(t), \quad (2)$$

where  $\mathbf{z}(t) = \mathbf{x}(t) - \mathbf{x}^*$ , and the  $N \times N$  matrix  $A$  is the sign-flipped Jacobian matrix of  $F$  at  $\mathbf{x}(t) = \mathbf{x}^*$ . Equation (2) is a multivariate Ornstein-Uhlenbeck (OU) process<sup>24,37</sup>, and  $\mathbf{x}^*$  is asymptotically stable in the absence of noise if and only if  $A$  is positive definite.

The covariance matrix in the equilibrium, corresponding to  $\mathbf{z}^* = (0, \dots, 0)^\top$ , is given as the solution to the Lyapunov equation given by

$$AC + CA^\top = BB^\top, \quad (3)$$

where  $C = (C_{ij})$  is the  $N \times N$  covariance matrix, and  $C_{ij}$  represents the covariance between  $z_i(t)$  and  $z_j(t)$ , which is equal to the covariance between  $x_i(t)$  and  $x_j(t)$ , at equilibrium<sup>37,38</sup>. The solution  $C$  is unique if the real part of all the eigenvalues of  $A$  is positive<sup>38</sup>.

Outcomes of the covariance matrix such as the standard deviation and correlation coefficient are often used as early warning signals for noisy multivariate dynamics. In practice, we need to estimate these quantities from samples. Therefore, we consider the sample variance of  $x_i(t)$ , which is a major early warning signal<sup>1,39-41</sup>, and its average over a given node set<sup>29,42</sup>, as candidates of early warning signals. The choice of the variance rather than the standard deviation is because of mathematical tractability. We emphasize that the rationale behind averaging the sample variance over nodes is that we may be then able to obtain a less fluctuating early warning signal than that calculated from a single node.

Assume that we observe  $L$  samples of  $x_i(t)$  from each node  $i$  in the given node set  $S$ . We denote by  $\hat{V}_i$  the unbiased sample variance of  $x_i(t)$  calculated from the  $L$  samples. Let us consider the average of  $\hat{V}_i$  over the  $n = |S|$  nodes in set  $S$  as an early warning signal. Without loss of generality, we assume that  $S = \{1, 2, \dots, n\}$ , where  $n \leq N$ . We denote this average by

$$\hat{V}_S = \frac{1}{n} \sum_{i=1}^n \hat{V}_i. \quad (4)$$

By assuming that  $z_{i,1}, \dots, z_{i,L}$  are i.i.d. and using  $E[z_{i,\ell}] = 0$ , we obtain

$$E[\hat{V}_S] = \frac{1}{n} \sum_{i=1}^n E[\hat{V}_i] = \frac{1}{n} \sum_{i=1}^n C_{ii} = \frac{1}{n} \text{Tr}(\bar{C}) = \frac{1}{n} \sum_{i=1}^n \lambda_i, \quad (5)$$

where  $E$  denotes the expectation,  $\text{Tr}$  denotes the trace,  $\bar{C}$  is the leading principal minor of order  $n$  of  $C$  (i.e., the submatrix of  $C$  composed of  $C_{ij}$  with  $i, j \in \{1, \dots, n\}$ ), and  $\lambda_i$  is the  $i$ th eigenvalue of  $C$ . As shown in Supplementary Note 1, we also obtain the variance of  $\hat{V}_S$ , denoted by  $\text{var}[\hat{V}_S]$ , as follows:

$$\begin{aligned} \text{var}[\hat{V}_S] &= \frac{2}{n^2(L-1)} \sum_{i=1}^n \sum_{j=1}^n (C_{ij})^2 \\ &= \frac{2}{n^2(L-1)} \text{Tr}(\bar{C}^2) \\ &= \frac{2}{n^2(L-1)} \sum_{i=1}^n \lambda_i^2. \end{aligned} \quad (6)$$

The coefficient of variation (CV), i.e., the standard deviation divided by the mean, of  $\hat{V}_S$ , which quantifies the relative uncertainty in the estimation of  $\hat{V}_S$ , is given by

$$CV = \sqrt{\frac{2}{L-1}} \frac{\sqrt{\sum_{i=1}^n \lambda_i^2}}{\sum_{i=1}^n \lambda_i}. \quad (7)$$

Equation (7) has a couple of implications. First, the CV decays according to  $\propto L^{-1/2}$  as the number of samples,  $L$ , increases, regardless of the node set  $S$ . This scaling corresponds to the central limit theorem. Second, in the case of a single node,  $CV = \sqrt{2/(L-1)}$  regardless of the node. Therefore, a large value of the sample covariance,  $\hat{V}_i$ , or its expectation,  $E[\hat{V}_i]$ , at a node  $i$  compared to at other nodes does not imply that  $\hat{V}_i$  is better than  $\hat{V}_j$ 's (with  $j \neq i$ ) as an early warning signal. A large signal carries a proportionately large amount of noise. This property also holds true when one uses the sample standard deviation,

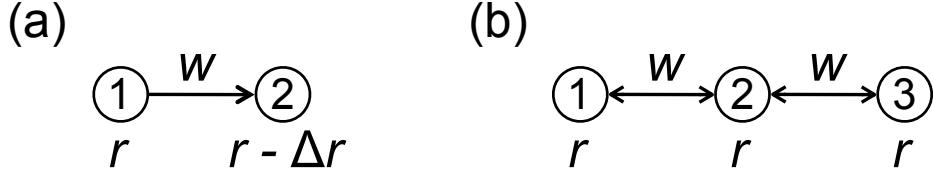


**Figure 1.** Schematic of two networks. (a) A network with  $N = 2$  nodes connected by a directed edge. (b) A symmetric chain network with  $N = 3$  nodes. The coupling strength is denoted by  $w$ . The stress given to each node is either  $r$  or  $r - \Delta r$ .

104 instead of the sample variance, of single nodes as early warning signal. Third, the CV with  $n \geq 2$  is always smaller than the CV  
 105 with  $n = 1$  (i.e.,  $\sqrt{2/(L-1)}$ ) unless all but one eigenvalues of  $\bar{C}$  are equal to 0. Note that this result holds true owing to  $\lambda_i \geq 0$   
 106  $\forall i$ , which follows from the fact that  $\bar{C}$  is a covariance matrix and therefore positive semidefinite. This result motivates us to use  
 107 the average of  $\hat{V}_i$  over nodes as opposed to  $\hat{V}_i$  at a single node with the aim of improving the performance of the early warning  
 108 signal. We will investigate this possibility in the following sections.

### 109 Coupled nonlinear dynamics on networks with two or three nodes

110 In this section, we analyze coupled nonlinear dynamics on networks with  $N = 2$  and  $N = 3$  nodes. Through this analysis, we  
 111 highlight relevance of multistage transitions, impact of averaging  $\hat{V}_i$  over nodes, heterogeneous amount of dynamical noise  
 112 given to different nodes, and uncertainty of early warning signals, among other things. We then propose a measure of the quality  
 113 of early warning signals in the form of  $\hat{V}_S$  and a method to select an optimal node set for constructing early warning signals.

#### 114 Two nodes connected by a directed edge

We consider a network composed of two nodes and a directed edge of weight  $w(\geq 0)$ ; see Fig. 1(a) for a schematic. We assume  
 that node 1 influences node 2 but not vice versa. We also assume that, as a bifurcation parameter, denoted by  $r$ , gradually  
 increases, node 1 undergoes a saddle-node bifurcation and that node 2 also undergoes a saddle-node bifurcation either almost at  
 the same time as node 1 or after  $r$  has further increased. The model is given by

$$dx_1(t) = f(x_1(t), r)dt + \sigma_1 dW_1(t), \quad (8)$$

$$dx_2(t) = [f(x_2(t), r - \Delta r) + w(x_1(t) + 1)]dt + \sigma_2 dW_2(t), \quad (9)$$

115 where  $\Delta r (\geq 0)$  is a constant,  $\sigma_1$  and  $\sigma_2$  are the intensities of dynamical noise applied to nodes 1 and 2, respectively, and  
 116  $f(x)$  satisfies the following conditions. First, we assume  $f(x, r) = r + x^2$  when  $r \leq 0$  and  $x \leq \sqrt{-r} + \Delta x$ , where  $\Delta x (> 0)$   
 117 is a small constant. This condition guarantees that, in the absence of coupling and dynamical noise, Eqs. (8) and (9) are  
 118 both the topological normal form of the saddle-node bifurcation<sup>43</sup>. In other words,  $dx/dt = f(x, r)$  with  $r < 0$  has a stable  
 119 equilibrium  $x^* = -\sqrt{-r}$  and an unstable equilibrium  $x^* = \sqrt{-r}$ , which collide at  $x^* = 0$  when  $r = 0$ . In Fig. 2, we show an  
 120 example bifurcation diagram of single-node deterministic dynamics given by  $dx/dt = f(x, r)$ . If  $\sigma_1 = 0$ , then  $x_1(t)$  undergoes  
 121 a saddle-node bifurcation at  $r = 0$  as  $r$  increases starting with a negative value. If  $\sigma_2 = 0$  and  $w = 0$ , then  $x_2(t)$  undergoes a  
 122 saddle-node bifurcation at  $r = \Delta r$ . Second, we assume that  $f(x, r)$  is continuous in terms of  $x$  and  $r$  for simplicity. Third, we  
 123 assume that  $f(c, r) = 0$  for  $\forall r \geq 0$  for a unique positive value of  $c$ , which is larger than  $\Delta x$ . This implies that, in the absence  
 124 of noise,  $x = c$  is the unique stable equilibrium after a node undergoes a saddle-node bifurcation as  $r$  gradually increases.  
 125 This assumption in combination with the continuity assumption for  $f(x, r)$  also implies that the stable equilibrium apart from  
 126  $x^* = -\sqrt{-r}$  persists for some  $r < 0$  although its position changes from  $x = c$  in general. Therefore, there are two stable  
 127 equilibria at least in some range of  $x < 0$  near  $x = 0$ , as shown in Fig. 2.

128 We assume that  $w > 0$  and consider this dynamical system in the range of bifurcation parameter  $r \in [-1, 0]$ , with  $(x_1, x_2)$   
 129 satisfying  $-1 \leq x_1, x_2 < 0$  in the absence of dynamical noise. In other words, we assume that  $x_1$  and  $x_2$  are both near the lower  
 130 stable equilibrium in Fig. 2. In this situation, the input that node 2 receives from node 1, i.e.,  $w(x_1 + 1)$ , is positive. To prevent  
 131 node 2 from transiting from its lower to the upper state through a saddle-node bifurcation earlier than node 1 when  $r$  gradually  
 132 increases, we assume that  $w \leq \Delta r$ , which guarantees that  $-\Delta r + w(x_1 + 1) \leq 0$ . Let us gradually increase  $r$  starting with  $r = -1$ .  
 133 Then,  $x_1$  jumps from 0 to  $c$  at  $r = 0$  via a saddle-node bifurcation. We distinguish between two cases depending on the change  
 134 in  $x_2$  right after the transition of node 1 from  $x_1 = 0$  to  $x_1 = c$ . If  $-\Delta r + w(c + 1) > 0$ , then  $x_2$  transits from  $x_2 = 0$  to  $x_2 = c$   
 135 immediately after  $x_1$  does without a further increase in  $r$  (i.e., at  $r = 0$ ). Otherwise,  $x_2$  does not transit at  $r = 0$ , and  $x_2$  does so  
 136 at a positive value of  $r$  if we further increase  $r$ . The latter case is a multistage transition<sup>28,29</sup>.

The lower equilibrium of the coupled dynamical system, which exists if and only if  $r \leq 0$  and is locally stable when  $r < 0$ ,

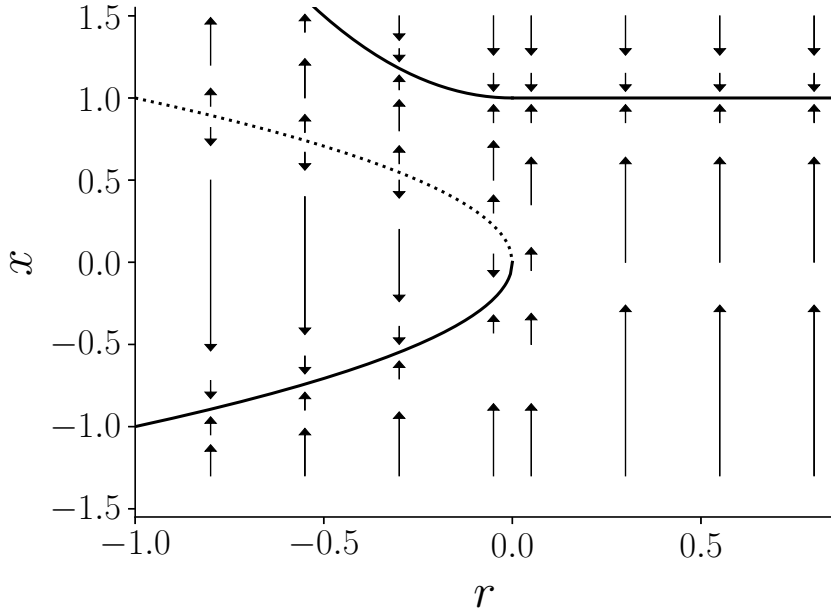


**Figure 2.** An example bifurcation diagram of single-node dynamics given by Eq. (8) without dynamical noise. The solid and dashed lines represent stable and unstable equilibria, respectively.

is given by

$$\mathbf{x}^* = \begin{pmatrix} x_1^* \\ x_2^* \end{pmatrix} = \begin{pmatrix} -\sqrt{-r} \\ -\sqrt{-r + \Delta r + w(\sqrt{-r} - 1)} \end{pmatrix}. \quad (10)$$

The linearized dynamics around  $\mathbf{x}^*$  is given by Eq. (2) with

$$A = \begin{pmatrix} -2x_1^* & 0 \\ -w & -2x_2^* \end{pmatrix}. \quad (11)$$

By combining Eqs. (3) and (11), we obtain

$$C_{11} = -\frac{\sigma_1^2}{4x_1^*}, \quad (12)$$

$$C_{12} = \frac{\sigma_1^2 w}{8x_1^*(x_1^* + x_2^*)}, \quad (13)$$

$$C_{22} = -\frac{\sigma_1^2 w^2}{16x_1^* x_2^*(x_1^* + x_2^*)} - \frac{\sigma_2^2}{4x_2^*}. \quad (14)$$

<sup>137</sup> Note that  $x_1^*$  and  $x_2^*$  are negative such that  $C_{11}$ ,  $C_{12}$ , and  $C_{22}$  are positive.

<sup>138</sup> Here we recall that  $E$  denotes the expectation, and we let  $\text{std}$  denote the standard deviation. Because  $x_1^* = 0^-$  as  $r \rightarrow 0^-$ , all <sup>139</sup> of  $C_{11}$ ,  $C_{12}$ , and  $C_{22}$  diverge as  $r \rightarrow 0^-$ . Therefore,  $E[\hat{V}_1]$ ,  $E[\hat{V}_2]$ , and  $E[\hat{V}_{\{1,2\}}]$ , which are equal to  $C_{11}$ ,  $C_{22}$ , and  $(C_{11} + C_{22})/2$ , <sup>140</sup> respectively, all diverge as  $r \rightarrow 0^-$  according to  $\propto (-r)^{-1/2}$ . However, we argue that this fact does not immediately imply that <sup>141</sup>  $\hat{V}_1$ ,  $\hat{V}_2$ , or  $\hat{V}_{\{1,2\}}$  is a high-quality early warning signal for the saddle-node bifurcation occurring at  $r = 0$  because  $\text{std}[\hat{V}_1]$ ,  $\text{std}[\hat{V}_2]$ , <sup>142</sup> and  $\text{std}[\hat{V}_{\{1,2\}}]$ , which are proportional to  $C_{11}$ ,  $\sqrt{C_{11}^2 + 2C_{12}^2 + C_{22}^2}$ , and  $C_{22}$ , respectively, also diverge.

<sup>143</sup> To investigate the quality of  $\hat{V}_1$ ,  $\hat{V}_2$ , and  $\hat{V}_{\{1,2\}}$  as early warning signals, we set  $w = 0.5$ ,  $\sigma_1 = 0.1$ ,  $L = 100$ , and used <sup>144</sup> three pairs of  $\Delta r$  and  $\sigma_2$  values, which we refer to as scenarios. In Fig. 3, we show  $E[\hat{V}_1]$ ,  $E[\hat{V}_2]$ ,  $E[\hat{V}_{\{1,2\}}]$ ,  $\text{std}[\hat{V}_1]$ ,  $\text{std}[\hat{V}_2]$ , <sup>145</sup> and  $\text{std}[\hat{V}_{\{1,2\}}]$  as we gradually increase  $r$  under the three scenarios. In Fig. 3(a), we show the results for the first scenario,

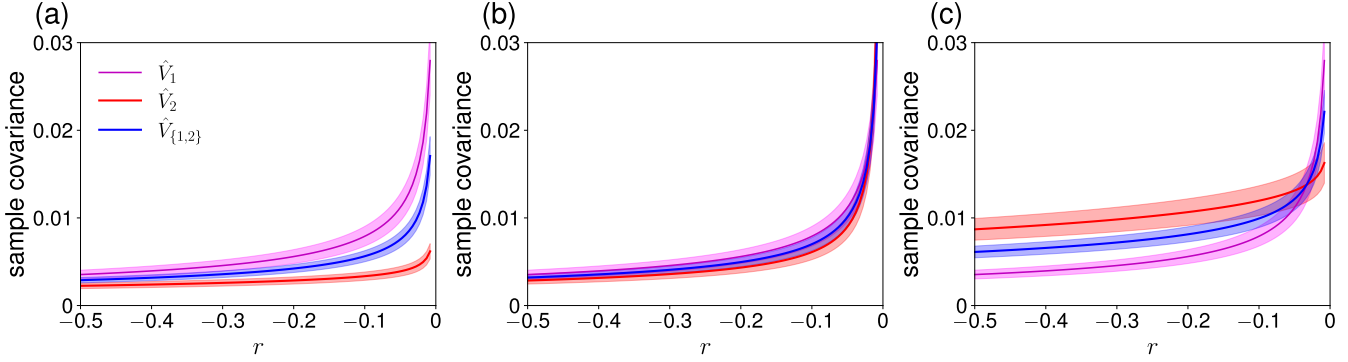


**Figure 3.** Early warning signals with different node sets in a network with  $N = 2$  nodes connected by a directed edge. The solid lines represent the mean. The shaded regions represent the standard deviation. We set  $w = 0.5$ ,  $\sigma_1 = 0.1$ , and  $L = 100$ . (a)  $(\sigma_2, \Delta r) = (0.1, 1)$ . (b)  $(\sigma_2, \Delta r) = (0.1, 0.5)$ . (c)  $(\sigma_2, \Delta r) = (0.2, 1)$ .

for which we set  $\Delta r = 1$  and  $\sigma_2 = \sigma_1 = 0.1$ . The solid lines represent the expected value of each early warning signal. The shaded area represents the mean  $\pm$  standard deviation. With these parameter values, when node 1 transits from  $x_1 = 0$  to  $x_1 = c$  at  $r = 0$ , node 2 is still far from the bifurcation point. This is because the input from node 1 to node 2, which is equal to  $w(x_1 + 1) \approx 0.5$ , is substantially smaller than  $-\Delta r (= 1)$  such that  $x_2$  approximately obeys  $dx_2 = (-0.5 + x^2)dt + \sigma_2 dW_2(t)$  near  $r = 0$ . Right after node 1 transits from  $x_1 = 0$  to  $x_1 = c$  at  $r = 0$ , the input from node 1 to node 2 jumps to  $w(x_1 + 1) \approx 0.5(c + 1)$ . Therefore, a multistage transition in which nodes 1 and 2 transit from their lower to the upper state at different  $r$  values occurs if  $0.5(c + 1) < 1$ , i.e.,  $0 < c < 1$ . Otherwise (i.e.,  $c \geq 1$ ), node 2 also transits from its lower to the upper state at  $r = 0$ . Regardless of whether or not a multistage transition occurs, Fig. 3(a) indicates that  $E[\hat{V}_1]$  is more sensitive to increases in  $r$  than  $E[\hat{V}_2]$  and  $E[\hat{V}_{\{1,2\}}]$ , and that  $\text{std}[\hat{V}_1]$  is larger than  $\text{std}[\hat{V}_2]$  and  $\text{std}[\hat{V}_{\{1,2\}}]$ . Therefore, it is not obvious which of  $\hat{V}_1$ ,  $\hat{V}_2$ , or  $\hat{V}_{\{1,2\}}$  is a better early warning signal.

To rank these different candidates of early warning signals, we define the following index. We measure each early warning signal's mean and standard deviation at  $r = -0.3$  and  $r = -0.1$ . We do so based on the premise that it is necessary to measure signals at least at two  $r$  values to estimate how responsive the signal is to the change in the environment, i.e.,  $r$ . As we explained in the “Theory” section,  $\hat{V}_1$ ,  $\hat{V}_2$ , and  $\hat{V}_{\{1,2\}}$  obey a normal distribution at equilibrium. Therefore, we measure a distance, denoted by  $d$ , between the normal distribution at  $r = -0.3$  and that at  $r = -0.1$  for each early warning signal. If  $d$  is large, it is relatively easy to tell the increase in the signal with relatively small uncertainty as  $r$  increases from  $-0.3$  to  $-0.1$ , approaching a tipping point. Therefore, we propose that an early warning signal attaining a larger  $d$  value is better. Although there are various measures of the separability of two normal distributions<sup>44</sup>, inspired by the  $t$ -statistic, we define

$$d = \frac{|\mu_1 - \mu_2|}{\sqrt{\text{var}_1 + \text{var}_2}}, \quad (15)$$

where  $\mu_1$  and  $\text{var}_1$  are the mean and variance of the normal distribution at  $r = -0.3$ , and  $\mu_2$  and  $\text{var}_2$  are those at  $r = -0.1$ . We show in Supplementary Note 2 that the results shown in the remainder of this section are robust with respect to the choice of the two  $r$  values for calculating  $d$ . Note that  $d$  can be small even if the mean of the early warning signal grows by a large amount between the two  $r$  values. This is the case when  $\text{var}_1$  or  $\text{var}_2$  is large, i.e., when the uncertainty of  $r$  is large. In this situation, tracking the early warning signal is relatively uninformative. In contrast, even if the absolute magnitude of the increase in the signal is small (i.e., small  $|\mu_1 - \mu_2|$ ), the signal provides a good early warning if the uncertainty of  $r$  is small.

We have found that  $d(\hat{V}_1) = 2.58$ ,  $d(\hat{V}_2) = 1.27$ , and  $d(\hat{V}_{\{1,2\}}) = 2.78$ . Therefore, we suggest that  $\hat{V}_1$  is a better early warning signal than  $\hat{V}_2$ . We emphasize that it is not because  $\hat{V}_1$  is larger than  $\hat{V}_2$  but because  $\hat{V}_1$  responds more strongly to an increase in  $r$  than  $\hat{V}_2$  does with relatively small uncertainty. Furthermore,  $\hat{V}_{\{1,2\}}$ , i.e., the average of  $\hat{V}_1$  and  $\hat{V}_2$ , realizes a larger value of  $d$  than  $\hat{V}_1$ . Therefore, we suggest that  $\hat{V}_{\{1,2\}}$  is a better early warning signal than  $\hat{V}_1$  and  $\hat{V}_2$ . This is intuitively because the averaging cancels out noise in the two signals, while  $\hat{V}_1$  and  $\hat{V}_2$  are not independent of each other due to the edge between nodes 1 and 2. We note that  $E[\hat{V}_{\{1,2\}}]$  is smaller than  $E[\hat{V}_1]$  (see Fig. 3(a)), challenging a natural idea of using single nodes or node sets with the largest variance as sentinel nodes.

We show in Fig. 3(b) the mean and standard deviation of the signals for the second scenario; we changed  $\Delta r$  from 1 to 0.5. In this scenario,  $x_2(t)$  always transits from its lower to the upper state immediately after node 1 does so at  $r = 0$ . This is because, when  $r \rightarrow 0^-$ , Eq. (8) implies that  $x_1(t) \rightarrow 0^-$  if we ignore the noise term, and  $r - \Delta r + w(x_1(t) + 1) \approx 0$  combined with Eq. (9) implies that  $x_2(t) \rightarrow 0^-$ . Therefore, even with a small  $c$  value, both nodes 1 and 2 sequentially transit from its

lower to the upper state at  $r = 0$ . Figure 3(b) indicates that  $E[\hat{V}_2]$  is responsive to increases in  $r$  to an extent similar to  $E[\hat{V}_1]$  is. The  $d$  values confirm this, i.e.,  $d(\hat{V}_1) = 2.58$ ,  $d(\hat{V}_2) = 2.50$ , and  $d(\hat{V}_{\{1,2\}}) = 3.40$ . Because the quality of  $\hat{V}_2$  is much better than in the first scenario, the average signal,  $\hat{V}_{\{1,2\}}$ , is substantially better than  $\hat{V}_1$  in terms of  $d$  in the present second scenario, while  $\hat{V}_{\{1,2\}}$  was only marginally better than  $\hat{V}_1$  in the first scenario.

In addition to different amounts of constant stress as parametrized by  $\Delta r$ , different nodes may be subject to different amounts of dynamical noise. We show in Fig. 3(c) the results for the third scenario, in which we set  $\Delta r = 1$  and  $\sigma_2 = 0.2$ . In this scenario, the saddle-node bifurcation for node 2 is delayed such that a multistage transition may occur, as in the first scenario. The difference to the first scenario is that, in the present scenario, node 2 receives a larger dynamical noise than node 1. Therefore,  $\hat{V}_2$  is noisier than  $\hat{V}_1$  and  $\hat{V}_{\{1,2\}}$ , which is apparent in Fig. 3(c). If we only measure the early warning signals at one  $r$  value (e.g.,  $r = -0.3$  or  $r = -0.1$ ), then one may be tempted to regard that  $\hat{V}_2$  is a better early warning signal than  $\hat{V}_1$  and  $\hat{V}_{\{1,2\}}$  because  $E[\hat{V}_2]$  is larger than  $E[\hat{V}_1]$  and  $E[\hat{V}_{\{1,2\}}]$ . However, this conclusion is erroneous for two reasons. First,  $\text{std}[\hat{V}_2]$  is larger than  $\text{std}[\hat{V}_1]$  and  $\text{std}[\hat{V}_{\{1,2\}}]$ . Second,  $\hat{V}_2$  is not much sensitive to the change in  $r$ , as Fig. 3(c) shows. In fact, we obtain  $d(\hat{V}_1) = 2.58$ ,  $d(\hat{V}_2) = 0.97$ , and  $d(\hat{V}_{\{1,2\}}) = 2.12$ . This result suggests that  $\hat{V}_1$  is a better signal than  $\hat{V}_2$  and  $\hat{V}_{\{1,2\}}$ . In this case, taking the average of  $\hat{V}_1$  and  $\hat{V}_2$  does not help because  $\hat{V}_2$  is too poor. Lessons from the analysis of the present scenario are that (i) a large signal value does not necessarily imply a better early warning signal and that (ii) it is sometimes better to exclude some nodes from the calculation of the early warning signal if those nodes are either only marginally responsive to the change in the bifurcation parameter or they carry larger fluctuations than other nodes.

### 190 **Chain with three nodes**

In this section, we consider three nodes of identical nonlinear dynamics, except possible differences in the noise strength, coupled as an undirected chain network with  $N = 3$  nodes. We show a schematic of the network in Fig. 1(b). Specifically, we consider the set of stochastic differential equations given by

$$dx_1 = [f(x_1) + w(x_2 + 1)] dt + \sigma_1 dW_1, \quad (16)$$

$$dx_2 = [f(x_2) + w(x_1 + 1) + w(x_3 + 1)] dt + \sigma_2 dW_2, \quad (17)$$

$$dx_3 = [f(x_3) + w(x_2 + 1)] dt + \sigma_3 dW_3, \quad (18)$$

where  $f(x)$  is given in the “Two nodes connected by a directed edge” section. If  $c$  is small enough and  $\sigma_1 = \sigma_2 = \sigma_3$ , node 2 transits from its lower to the upper state earlier than nodes 1 and 3 as  $r$  ( $\geq -1$ ) increases from a negative value because node 2 receives positive input from nodes 1 and 3 while node 1 and 3 each receive input solely from node 2.

When  $-1 \leq r \leq 0$ , the equilibrium in the absence of noise satisfying  $x_1^*, x_2^*, x_3^* < 0$  is a solution of

$$r + (x_1^*)^2 + w(x_2^* + 1) = 0, \quad (19)$$

$$r + (x_2^*)^2 + 2w(x_1^* + 1) = 0, \quad (20)$$

and  $x_3^* = x_1^*$ . If we ignore the dynamical noise, the first saddle-node bifurcation, which is the transition of node 2 from its lower to the upper state, occurs at  $r = r_c$ , where  $r_c$  satisfies  $0 > r_c > r_c'' \equiv 2w[-(w+1) + \sqrt{w(w+1)}]$ , as  $r$  gradually increases from  $r = -1$ . At  $r = r_c$ , the two parabolas given by Eqs. (19) and (20) are tangent to each other. See Supplementary Note 3 for the derivation including that of the uniqueness of the stable solution satisfying  $x_1^* (= x_3^*) < 0$  and  $x_2^* < 0$  when  $r \leq r_c$ . We set  $w = 0.05$ , which leads to  $r_c \approx r_c'' \approx -0.082$ . Therefore, we calculate the  $d$  values at  $r = -0.3$  and  $-0.1$  as we did in the “Two nodes connected by a directed edge” section. We show in Supplementary Note 2 that the following results are reasonably robust against variation in the two  $r$  values.

We obtain the mean and standard deviation of the early warning signals, and then  $d$ , as follows. Equations (16), (17), and (18) lead to

$$A = \begin{pmatrix} -2x_1^* & -w & 0 \\ -w & -2x_2^* & -w \\ 0 & -w & -2x_1^* \end{pmatrix}. \quad (21)$$

To facilitate further analyses, we assume  $\sigma_1 = \sigma_3$ . Then, by substituting Eq. (21) and  $B = \text{diag}(\sigma_1, \sigma_2, \sigma_1)$ , which is by

definition the diagonal matrix whose diagonal entries are  $\sigma_1$ ,  $\sigma_2$ , and  $\sigma_1$  in this order, into Eq. (3), we obtain

$$C_{11} = C_{33} = \frac{-4x_1^*x_2^*(x_1^* + x_2^*)\sigma_1^2 + w^2[(2x_1^* + x_2^*)\sigma_1^2 - x_1^*\sigma_2^2]}{8x_1^*(2x_1^*x_2^* - w^2)(x_1^* + x_2^*)}, \quad (22)$$

$$C_{12} = C_{23} = \frac{w(x_2^*\sigma_1^2 + x_1^*\sigma_2^2)}{4(2x_1^*x_2^* - w^2)(x_1^* + x_2^*)}, \quad (23)$$

$$C_{13} = -\frac{w^2(x_2^*\sigma_1^2 + x_1^*\sigma_2^2)}{8x_1^*(2x_1^*x_2^* - w^2)(x_1^* + x_2^*)}, \quad (24)$$

$$C_{22} = \frac{-2x_1^*x_2^*(x_1^* + x_2^*)\sigma_2^2 + w^2x_2^*(-\sigma_1^2 + \sigma_2^2)}{4x_2^*(2x_1^*x_2^* - w^2)(x_1^* + x_2^*)}. \quad (25)$$

201 By substituting Eqs. (22)–(25) into Eqs. (5) and (6), we obtain the mean and standard deviation of each early warning signal for  
202 any node set  $S$ . Because  $\hat{V}_1$  and  $\hat{V}_3$  obey the same normal distribution, we obtain  $E[\hat{V}_{\{1,3\}}] = E[(\hat{V}_1 + \hat{V}_3)/2] = E[\hat{V}_1] = E[\hat{V}_3]$ .  
203 We also obtain  $\text{std}[\hat{V}_{\{1,3\}}] = (C_{11} + 2C_{13} + C_{33})/[2(L-1)] = \text{std}[\hat{V}_1] \times \frac{1+\text{Corr}}{2}$ , where  $\text{Corr}$  is the Pearson correlation coefficient  
204 between  $x_1(t)$  and  $x_3(t)$  in the equilibrium. Therefore,  $\text{std}[\hat{V}_{\{1,3\}}]$  is smaller than  $\text{std}[\hat{V}_1]$  unless  $x_1(t)$  and  $x_3(t)$  are perfectly  
205 correlated, which does not happen because they are subjected to independent Wiener processes  $dW_1(t)$  and  $dW_3(t)$ . Therefore,  
206  $\hat{V}_{\{1,3\}}$  is always better than  $\hat{V}_1$  and  $\hat{V}_3$  for this model. In addition, due to the assumed symmetry between nodes 1 and 3,  
207  $S = \{1,2\}$ ,  $\{1,3\}$ , and  $\{1,2,3\}$  exhaust all possibilities of combining multiple nodes' signals into one early warning signal.  
208 Therefore, it suffices to compare the performance of  $\hat{V}_2$ ,  $\hat{V}_{\{1,2\}}$ ,  $\hat{V}_{\{1,3\}}$ , and  $\hat{V}_{\text{all}} \equiv (\hat{V}_1 + \hat{V}_2 + \hat{V}_3)/3$ , i.e.,  $\hat{V}_S$  with  $S = \{1,2,3\}$ .

209 We set  $\sigma_2 = 0.1$  and  $L = 100$ , and consider three values of  $\sigma_1$ . In the first scenario, we set  $\sigma_1 = \sigma_2 = 0.1$ . For this case,  
210 we show the mean and standard deviation of  $\hat{V}_2$ ,  $\hat{V}_{\{1,2\}}$ ,  $\hat{V}_{\{1,3\}}$ , and  $\hat{V}_{\text{all}}$  as a function of  $r$  in Fig. 4(a). Note that the result for  
211  $\hat{V}_1$  is the same as that for  $\hat{V}_{\{1,3\}}$  except that  $\text{std}[\hat{V}_1]$  is  $2/(1+\text{Corr})$  ( $> 1$ ) times larger than  $\text{std}[\hat{V}_{\{1,3\}}]$ . It is not straightforward  
212 to tell from Fig. 4(a) which signal is better than others. However, we expect that  $\hat{V}_2$  provides a better early warning signal  
213 than  $\hat{V}_1$  because the transition of node 2 from the lower to the upper state as  $r$  increases from  $r \approx -0.5$  is more impending  
214 than the transition of nodes 1 and 3. In fact, we obtain  $d(\hat{V}_1) = 3.52$ ,  $d(\hat{V}_2) = 4.72$ ,  $d(\hat{V}_{\{1,2\}}) = 5.84$ ,  $d(\hat{V}_{\{1,3\}}) = 4.97$ , and  
215  $d(\hat{V}_{\text{all}}) = 6.77$ , verifying this prediction. Furthermore, it is the best to use  $\hat{V}_{\text{all}}$ , i.e., the average of the sample covariance over all  
216 nodes.

217 In the second scenario, we set  $\sigma_1 = 0.7$  such that nodes 1 and 3 receive larger dynamical noise than node 2. We show the  
218 behavior of the early warning signals in this case in Fig. 4(b). The figure indicates that the mean magnitude of any signals  
219 including  $\hat{V}_1$  (i.e.,  $\hat{V}_{\{1,2\}}$ ,  $\hat{V}_{\{1,3\}}$ , and  $\hat{V}_{\text{all}}$ ) is much larger than that of  $\hat{V}_2$ . However, this phenomenon does not imply that it is better  
220 to use a signal including  $\hat{V}_1$  because the enhanced signal size owes to the increased amount of dynamical noise. We obtain  
221  $d(\hat{V}_1) = 3.49$ ,  $d(\hat{V}_2) = 5.49$ ,  $d(\hat{V}_{\{1,2\}}) = 3.74$ ,  $d(\hat{V}_{\{1,3\}}) = 4.93$ , and  $d(\hat{V}_{\text{all}}) = 5.10$ . Therefore, we suggest that we should only  
222 use node 2 as early warning signal under the present scenario because  $\hat{V}_2$  is the least affected by the dynamical noise. Note that  
223 the magnitude of  $\hat{V}_2$  in the present scenario is similar to that in the first scenario (see Fig. 4(a)).

224 In the third scenario, we set  $\sigma_1 = 0.015$  such that node 2 receives large dynamical noise than nodes 1 and 3. We show the  
225 behavior of the early warning signals in this case in Fig. 4(c). We find that  $E[\hat{V}_2]$  is much larger than  $E[\hat{V}_{\{1,3\}}]$  ( $= E[\hat{V}_1]$ ), which  
226 does not use  $\hat{V}_2$ . Note that, the magnitude of  $\hat{V}_2$  is similar to that in the last two scenarios because we kept  $\sigma_2 = 0.1$  in all the  
227 three scenarios. We obtain  $d(\hat{V}_1) = 4.50$ ,  $d(\hat{V}_2) = 4.69$ ,  $d(\hat{V}_{\{1,2\}}) = 4.77$ ,  $d(\hat{V}_{\{1,3\}}) = 6.08$ , and  $d(\hat{V}_{\text{all}}) = 4.84$ . Therefore, we  
228 suggest that  $\hat{V}_{\{1,3\}}$  is the best early warning signal under the present scenario. In the second and third scenarios, the best early  
229 warning signal turns out to be the one having the smallest mean magnitude at both  $r = -0.3$  and  $r = -0.1$ .

### 230 Numerical results for larger networks and various dynamical systems

231 We propose to use the node set  $S$  maximizing  $d$  as the sentinel node set from which we calculate the early warning signal,  $\hat{V}_S$ .  
232 In the networks with two or three nodes analyzed in the “Coupled nonlinear dynamics on networks with two or three nodes”  
233 section, the maximizers of  $d$  are composed of nodes with small dynamical noise (i.e., small  $\sigma_i$ ). However, in networks with  
234 larger numbers of nodes, it may not be the best to select nodes with small dynamical nodes. It is because  $x_i$ 's of these nodes  
235 may be strongly correlated with each other, which typically occurs when these nodes are closely located in the network. In this  
236 case, averaging  $\hat{V}_i$  over these nodes, which yields  $\hat{V}_S$ , does not help much to reduce the fluctuation, potentially making this  $\hat{V}_S$  a  
237 poor early warning signal. Therefore, to test the performance of our method to select the sentinel node set in networks with  
238 larger numbers of nodes, we carry out numerical simulations with different networks and dynamical systems in this section.

### 239 Setup for numerical simulations

240 We use six undirected and unweighted networks with  $N$  nodes and denote a network's adjacency matrix by  $(w_{ij})$ , with  $w_{ii} = 0$   
241 and  $w_{ij} = w_{ji} \in \{0, 1\} \forall i, j \in \{1, \dots, N\}$ .

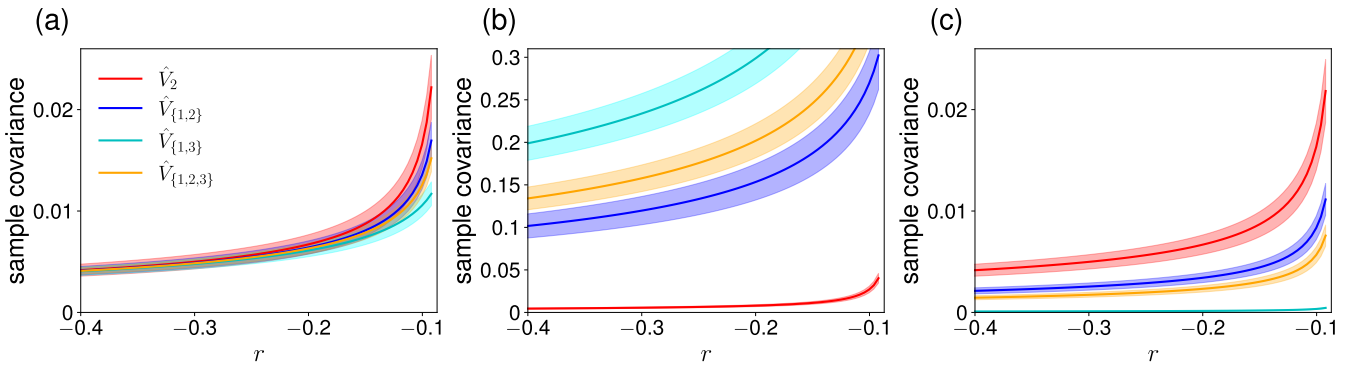


**Figure 4.** Early warning signals with different node sets in the undirected chain network with  $N = 3$  nodes. We set  $w = 0.05$ ,  $\sigma_2 = 0.1$ , and  $L = 100$ . (a)  $\sigma_1 = 0.1$ . (b)  $\sigma_1 = 0.7$ . (c)  $\sigma_1 = 0.015$ .

242 Our theory requires the covariance matrix,  $C$ , or at least its eigenvalues, estimated at two values of the bifurcation parameter.  
243 In the previous sections, we theoretically calculated  $C$  by linearizing the original dynamics around the equilibrium and solving  
244 the Lyapunov equation given by Eq. (3). However, to know matrix  $A$  in Eq. (3), we need to know the term driving the dynamics  
245 of the node, i.e., the derivative of  $F$  in Eq. (1), which depends on the single node's intrinsic dynamics and form of the coupling  
246 between nodes. However, we usually do not have access to such detailed information given empirical data, while estimating  
247 them from observed data is an active research field (e.g., Ref.<sup>23</sup>). Therefore, we use the sample covariance matrix as an  
248 estimator of  $C$ . This choice is for simplicity, and there are better estimators of the covariance matrix that are useful especially  
249 when the number of samples,  $L$ , is small relative to the number of variables,  $N$ <sup>45</sup>; we will discuss this limitation of the present  
250 study in the “Discussion” section.

251 **Results for the coupled double-well model**

We first consider a coupled double-well model on networks with dynamical noise given by

$$dx_i = \left[ -(x_i - r_1)(x_i - r_2)(x_i - r_3) + D \sum_{j=1}^N w_{ij} x_j + u_i \right] dt + \sigma_i dW_i, \quad i \in \{1, \dots, N\}. \quad (26)$$

252 Equation (26) represents dynamics of species abundance<sup>25</sup> or climates in interconnected regions<sup>26</sup>. Parameters  $r_1$ ,  $r_2$ , and  $r_3$   
253 control the location of the equilibria and satisfy  $r_1 < r_2 < r_3$ ;  $D$  ( $\geq 0$ ) is the strength of coupling between nodes, and  $u_i$  is a  
254 constant stress given to the  $i$ th node, equivalent to  $-\Delta r$  in Eq. (9). When  $D$  or  $u_i \forall i$  is sufficiently small,  $\mathbf{x} = (x_1, \dots, x_N)^\top$  in  
255 which all the nodes are in their lower state near  $r_1$  is the unique stable equilibrium. In contrast, when  $D$  or  $u_i \forall i$  is sufficiently  
256 large,  $\mathbf{x}$  in which all the nodes are in their upper state near  $r_3$  is the unique stable equilibrium. In between, we initially set all  
257 the nodes in their lower state at the start of each simulation, and as one gradually increases  $D$  or  $u_i$ , all nodes may flip to the  
258 upper stable state at once or in multiple stages<sup>28,29</sup>.

259 For this system, we numerically assess the performance of the variance of a single node or its average over the nodes in  
260 set  $S$  as early warning signal to anticipate the first transition from the lower state to the upper state. We use either  $u_i$  or  $D$  as  
261 the bifurcation parameter in a given sequence of simulations. If the bifurcation parameter is  $u_i$ , we started with  $D = 0.05$  and  
262  $u_i = u = 0 \forall i$  and gradually increased  $u$  until the first transition occurs (see the Methods section for the precise definition of the  
263 transition and parameter values for the numerical simulations). We computed the covariance matrix at reasonably separated  
264 two values of  $u$ , denoted by  $u^{(1)}$  and  $u^{(2)}$  (see the Methods section for details). At each of  $u = u^{(1)}$  and  $u = u^{(2)}$ , we collected  
265  $L = 100$  samples of each  $x_i$ ,  $i \in S$  and calculated  $d$  using Eq. (15). As a demonstration, we show how noisy early warning  
266 signals gradually increase as we gradually increase  $u$  in one series of simulations in Fig. 5. When we select  $n = 5$  nodes  
267 uniformly at random, the sample covariance averaged over the nodes in  $S$  (i.e.,  $\hat{V}_S$ ) gradually increases until the first node  
268 transits from its lower to the upper state (see the orange line). When we use the set of  $n = 5$  nodes maximizing  $d$ , the sensitivity  
269 of  $\hat{V}_S$  to the increase in  $u$  is notably larger near the first tipping point (see the blue line). Therefore, the maximizer of  $d$  provides  
270 an apparently better early warning signal than a uniformly randomly selected node set.

271 We assessed the performance of the sample covariance averaged over the nodes in  $S$  using the Kendall's  $\tau$ , which is  
272 conventionally used<sup>13</sup>. We evaluated  $S$  with  $n = \{1, 2, 3, 4, 5\}$  nodes and also the  $S$  composed of all  $N$  nodes, which refer to as  
273 “all”, as a control. We exhaustively examined all possible  $S$  with  $n = 1$  or  $n = 2$  and uniformly randomly sampled 5000 sets of  
274  $S$  for each  $n \in \{3, 4, 5\}$  due to a large number of combinations. In Supplementary Note 4, we also provide a stopping criterion  
275 and a numerical demonstration when one wants to explore  $S$  with  $n > 5$  nodes for better solutions (i.e.,  $S$  with larger  $d$  values).

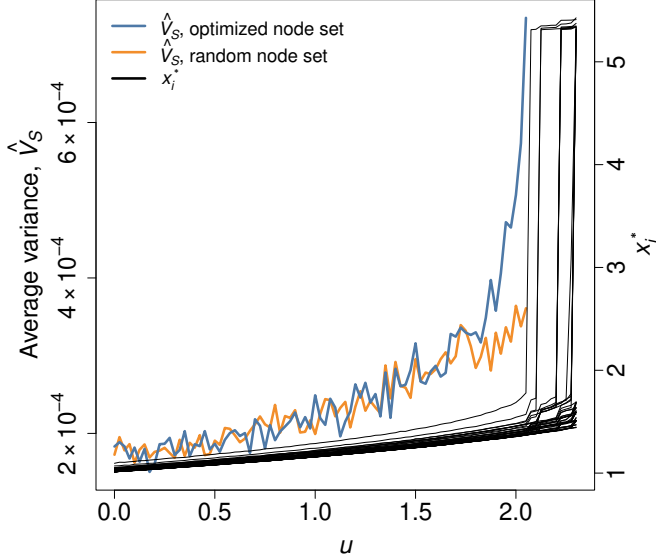


**Figure 5.** Early warning signal,  $\hat{V}_S$ , for the maximizer of  $d$  (blue line) and a set of nodes selected uniformly at random (orange line). Both sentinel node sets are composed of  $n = 5$  nodes. We also show  $x_i^*$  for each node at each value of  $u$ . We used the coupled double-well dynamics on a BA network with  $N = 50$  nodes and gradually increased  $u$ .

276 We show the results of one set of simulations on the Barabási-Albert (BA) model network with 50 nodes and average degree  
 277  $\langle k \rangle = 3.88$  in Fig. 6. We gradually increased  $u$  as the bifurcation parameter. Figure 6(a) shows the relationship between the  
 278 Kendall's  $\tau$  and  $d$  when the early warning signal is the variance of a single  $x_i$ . Each symbol corresponds to a node. We find  
 279 that the node maximizing  $d$ , indicated by the intersection of the two dashed lines, is the third best performer in terms of  $\tau$ . At  
 280 each value of  $n \in \{2, 3, 4, 5\}$ , the maximizer of  $d$  is not the top performer in terms of  $\tau$  but is a reasonably good performer (see  
 281 Figs. 6(b)–(e)). For example, the pair of nodes attaining the largest  $d$ , corresponding to the symbol at the intersection of the two  
 282 dashed lines in Fig. 6(b), provides the eighth best early warning signal among all the  $N(N - 1)/2 = 1225$  pairs of nodes. At  
 283 each value of  $n \in \{1, \dots, 5\}$ , we find that  $\tau$  and  $d$  are positively correlated; the Pearson correlation coefficient between  $\tau$  and  
 284  $d$  is equal to 0.42, 0.46, 0.45, 0.44, and 0.43 for  $n = 1, 2, 3, 4$ , and 5, respectively. It should also be noted that both  $d$  and  $\tau$   
 285 generally increase as  $n$  increases. When all nodes are used,  $d$  and  $\tau$  are the largest (see Fig. 6(f)). Therefore, in the present  
 286 case, using all the nodes is a better choice than using particular combinations of  $n \leq 5$  nodes. However, a reasonably large  $\tau$   
 287 is attained only using  $n \leq 5$  nodes if we choose appropriate node sets based on  $d$ . One can find  $S$  that maximizes  $d$  only by  
 288 observing the covariance matrix at two bifurcation parameter values.

289 We quantified the performance of the optimized node set, i.e., the node set that maximizes  $d$  at each value of  $n$ , using  $p_1$   
 290 and  $p_2$ . For a given  $n$ , we define  $p_1$  as twice the fraction of node sets whose  $\tau$  is larger than that for the optimized node set.  
 291 We note that  $0 \leq p_1 \leq 2$ . We define  $p_2$  as  $(\tau_{\max} - \tau^*)/(\tau_{\max} - \langle \tau \rangle)$ , where  $\langle \tau \rangle$  is the average of  $\tau$  over all the node sets with  
 292  $n$  nodes examined,  $\tau_{\max}$  is the largest (i.e., best)  $\tau$  value among the node sets with  $n$  nodes examined, and  $\tau^*$  is the  $\tau$  value  
 293 realized by the maximizer of  $d$  with  $n$  nodes. Although we have assumed that a larger positive  $\tau$  is better, the definition of  $p_1$   
 294 and  $p_2$  are similar when the nodes transit from their upper to lower states through tipping points and therefore a larger negative  
 295  $\tau$  implies a better performance of an early warning signal (Supplementary Note 5). If the maximizer of  $d$  is the best node set,  
 296 realizing the largest  $\tau$ , then both  $p_1$  and  $p_2$  are equal to 0 and the smallest. Smaller  $p_1$  and  $p_2$  values are better. If half the node  
 297 sets are better than the maximizer of  $d$ , meaning that the maximizer of  $d$  is no better than a uniformly random pick, then we  
 298 obtain  $p_1 = 1$ . Similarly,  $p_2 = 1$  is equivalent to  $\tau^* = \langle \tau \rangle$ , implying that the maximizer of  $d$  is no better than a random pick. If  
 299 the maximizer of  $d$  is the worst performer, we obtain  $p_1 = 2$  and a value of  $p_2$  larger than 1.

300 We show in Fig. 7(a) the  $p_1$  and  $p_2$  values for the double-well dynamics on the BA network with  $n \in \{1, \dots, 5\}$ . Each  
 301 small symbol represents the  $p_1$  and  $p_2$  values for a single series of simulations in which we gradually increased the value of  $u$   
 302 towards the first transition. Figure 6 shows the relationship between  $\tau$  and  $d$  in one of the 50 series of simulations whose results  
 303 are shown in Fig. 7(a). The larger symbols in Fig. 7 indicate the average over the 50 series of simulations. We find that the  
 304 optimizer of  $d$  is not a top but reasonably good performer because the  $p_1$  and  $p_2$  values are substantially smaller than 1 in most  
 305 runs. The performance of the maximizer of  $d$  relative to that of uniformly randomly selected node sets with the same number of  
 306 nodes,  $n$ , degrades as  $n$  increases.

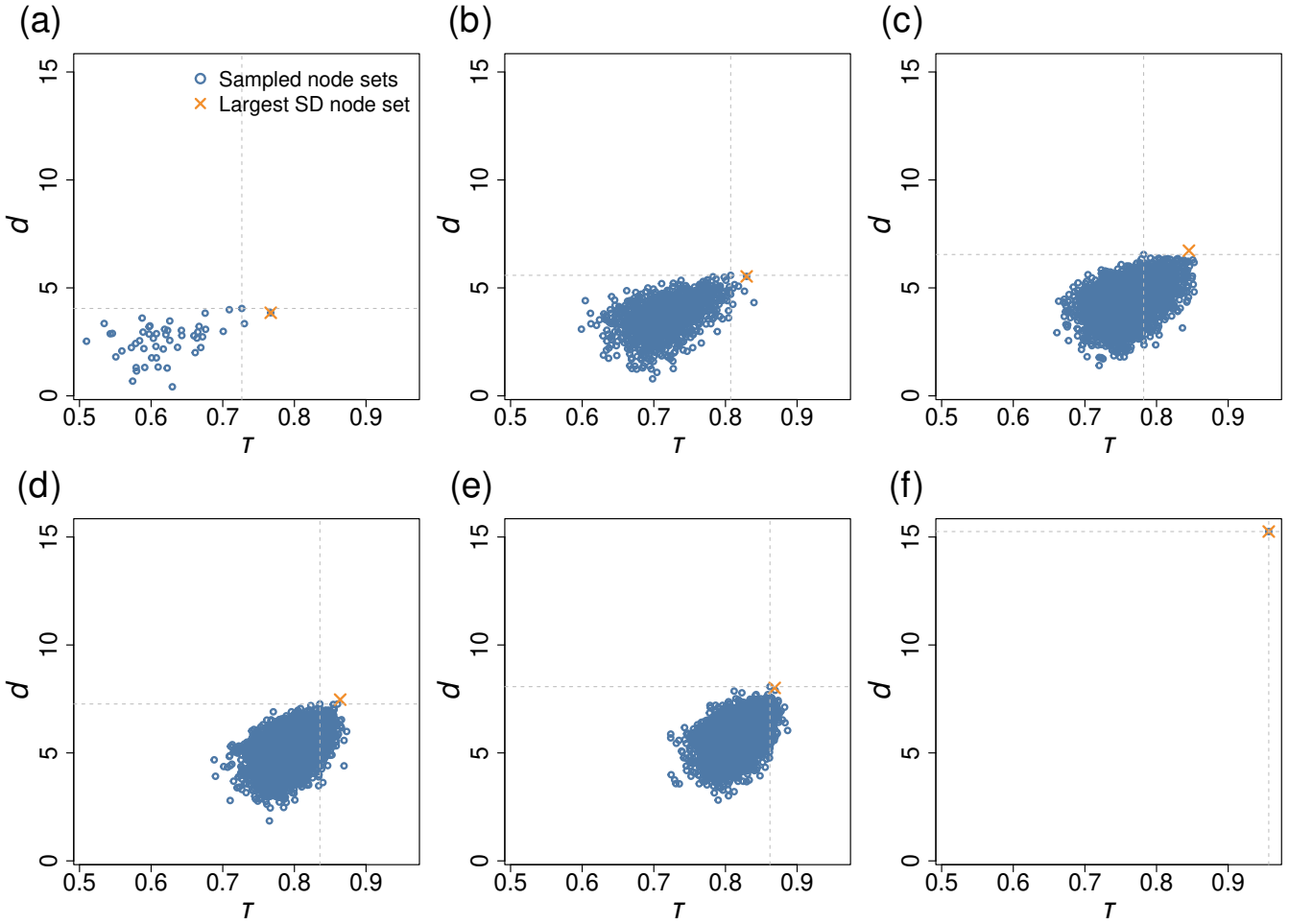


**Figure 6.** Relationships between the Kendall's  $\tau$  and  $d$  before the first major transition in the coupled double-well dynamics on a BA network with  $N = 50$  nodes. We gradually increased  $u$ . We considered node sets  $S$  with  $n \in \{1, 2, 3, 4, 5, N\}$  nodes. (a)  $n = 1$ . (b)  $n = 2$ . (c)  $n = 3$ . (d)  $n = 4$ . (e)  $n = 5$ . (f)  $n = N$ . The  $\tau$  and  $d$  values for the node set maximizing  $d$  for each  $n$  value are highlighted by the dashed lines. The cross represents “Large SD”, i.e., the node set comprised of the  $n$  nodes with the largest sample standard deviation of  $x_i(t)$ .

307 **Robustness of node set optimization under different heterogeneity scenarios, networks, dynamical systems, and other**  
 308 **factors**

309 To examine the generality of the effectiveness of the node set optimization, we ran simulations, assessed the performance of the  
 310 early warning signals in terms of the Kendall's  $\tau$ , and calculated  $p_1$  and  $p_2$  for the following variations. First, we have assumed  
 311 that all nodes are homogeneous except with regard to the position in the network. However, as we examined with Figs. 3(a) and  
 312 (b), different nodes may have different propensity to tip, yielding a multistage transition for the entire system. To examine this  
 313 case, we set  $u_i = u + \Delta u_i$  in Eq. (26), where  $\Delta u_i$  independently obeys the uniform density on  $[-0.25, 0.25]$ . We continue to use  
 314  $u$  as the bifurcation parameter. A node with large  $u_i$  tends to transit from its lower state to the upper state earlier as  $u$  gradually  
 315 increases. Note that a heterogeneous distribution of  $u_i$  makes it more difficult to find a good node set  $S$  only from the information  
 316 on the network structure. We show the  $p_1$  and  $p_2$  values when  $u_i$  is heterogeneous and  $\sigma_i$  is homogeneous in Fig. 7(b). The  
 317 results are qualitatively the same as those for the case in which both  $u_i$  and  $\sigma_i$  are homogeneous (see Fig. 7(a)). Separately, we  
 318 also consider the case in which both the node stress  $u_i$  and the strength of the dynamical noise  $\sigma_i$  are heterogeneous. We set  
 319  $\sigma_i = \sigma + \Delta \sigma_i$ , where  $\sigma = 0.05$ , and  $\Delta \sigma_i$  independently obeys the uniform density on  $[-0.9\sigma, 0.9\sigma]$ . We show  $p_1$  and  $p_2$  for  
 320 this case in Fig. 7(c). The results are qualitatively the same as those when both  $u_i$  and  $\sigma_i$  are homogeneous (Fig. 7(a)) and when  
 321 only  $u_i$  is heterogeneous (Fig. 7(b)).

322 Second, we have considered six networks including the BA model, three of which are model networks and the other three  
 323 are empirical networks (see Methods for the networks). Third, we have considered four dynamical system models on networks  
 324 including the coupled double-well dynamics; the other three dynamics are a model of mutualistic interaction dynamics among

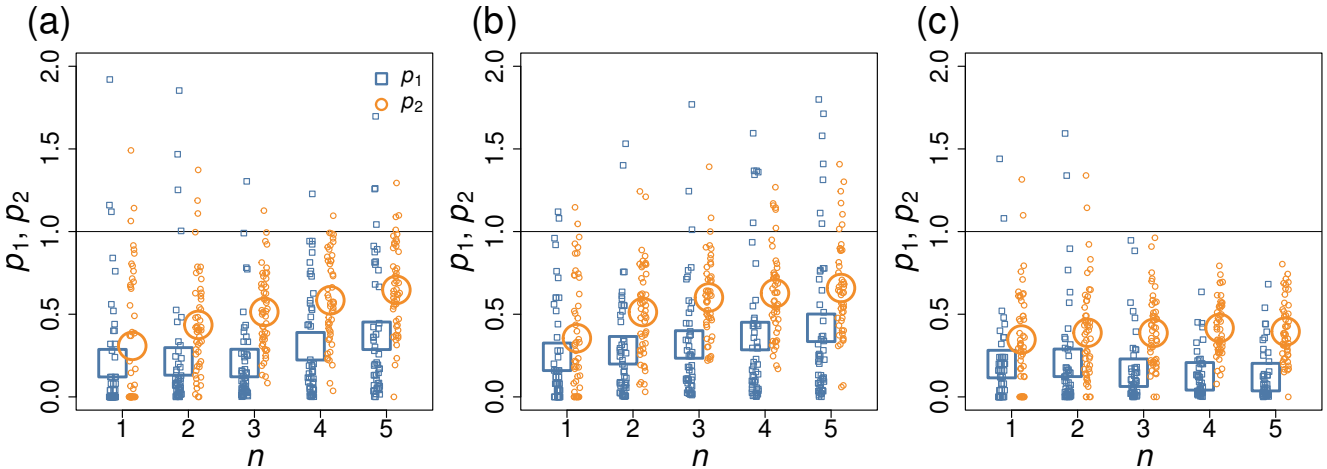


**Figure 7.** Performance of the optimized node set in anticipating the tipping point in the double-well dynamics on the BA model network with  $N = 50$  nodes. (a) Homogeneous stress and homogeneous noise. (b) Heterogeneous stress and homogeneous noise. (c) Heterogeneous stress and heterogeneous noise. The smaller symbols show the  $p_1$  and  $p_2$  values for the individual series of simulations. The larger symbols show the average over 50 series of simulations.

species<sup>46</sup>, a gene regulatory system governed by the Michaelis-Menten equation<sup>46</sup>, and the deterministic approximation of the susceptible-infectious-susceptible (SIS) model on networks<sup>47</sup>. These four models of dynamics are diverse in the sense that the SIS model shows a transcritical bifurcation to mark the onset of epidemic spreading, while the other three models show saddle-node bifurcations. In addition, we started the mutualistic interaction and gene regulatory dynamics from the upper state for each node and gradually decreased the bifurcation parameter value, which is the opposite to the case of the double-well and SIS dynamics. This is because the loss of resilience such as species loss in mutualistic dynamics and cell death in gene regulatory dynamics is of a practical concern for these dynamical systems<sup>46</sup>. Fourth, we also varied  $D$  instead of  $u$  as bifurcation parameter until the first bifurcation occurs. For the SIS model, we only considered an equivalent to  $D$ , which is the infection rate parameter, but not  $u$  because introducing and varying  $u$  is unrealistic for the SIS model; see Methods for the discussion.

We show the  $p_1$  and  $p_2$  values for  $n \in \{1, \dots, 5\}$ , the three different scenarios for  $u_i$  and  $\sigma_i$  (i.e., constant across all nodes or heterogeneous), two networks, four different dynamical systems, and two different bifurcation parameters (i.e.,  $u$  or  $D$ ) in Fig. 8. Each figure panel contains the average of  $p_1$  and  $p_2$  over 50 series of simulations for the three scenarios of heterogeneity (i.e., both  $u_i$  and  $\sigma_i$  are homogeneous, only  $u_i$  is heterogeneous, and both of them are heterogeneous) for one network and one dynamical system. Note that Fig. 8(a) is for the double-well dynamics on the BA network, corresponding to Figs. 6 and 7. We find that the node set based on the largest  $d$  value performs reasonably well for the two networks (see Figs. 8(a)–(g) for the BA network and Figs. 8(h)–(n) for the Chesapeake Bay carbon flow network) and for all the four models of dynamics. The node set maximizing  $d$  tends to work better relative to uniformly randomly picked node sets, yielding smaller  $p_1$  and  $p_2$  values, when  $u_i$  and  $\sigma_i$  are both heterogeneous across the nodes (shown by the dotted lines) than when either  $u_i$  or  $\sigma_i$  is homogeneous (shown by the solid and dashed lines). This is presumably because the proposed method actively discards nodes with high intrinsic noise by comparing the distribution of the signal variance at two values of the bifurcation parameter. The node set maximizing  $d$  tends to work better relative to uniformly random node sets with the same number of nodes,  $n$ , when  $n$  is smaller. However, even at  $n = 5$ , the  $p_1$  and  $p_2$  values are at most approximately 0.7 and much smaller in a majority of cases. The results are qualitatively the same for the other four networks, with a caveat that the maximizer of  $d$  performs poorly for the gene regulatory dynamics model on some networks (see Supplementary Note 6).

We also carried out the following robustness tests.

Our choice of the two bifurcation parameter values at which we sample the covariance matrix and then calculate  $d$  (see Methods for the definition of the two bifurcation parameter values) has been arbitrary. We used one bifurcation parameter value close to the start of each series of simulation and the other value close to the first tipping point, regardless of the type of bifurcation. This is because, with this choice, the difference between  $\mu_1$  and  $\mu_2$ , which is the numerator of  $d$  (see Eq. (15)), is larger than when the two bifurcation parameter values are closer. Then, the contrast of  $d$  for different choices of  $S$  may be larger, potentially helping to single out the  $S$  that maximizes  $d$ . To test the robustness of our results with respect to the choice of the two bifurcation parameter values, we measured  $p_1$  and  $p_2$  for various pairs of the bifurcation parameter value, which are different in terms of the separation between the two values and the closeness to the first tipping point. For the three scenarios for  $u_i$  and  $\sigma_i$  (i.e., constant across all nodes or heterogeneous), six networks, four dynamical systems, and two bifurcation

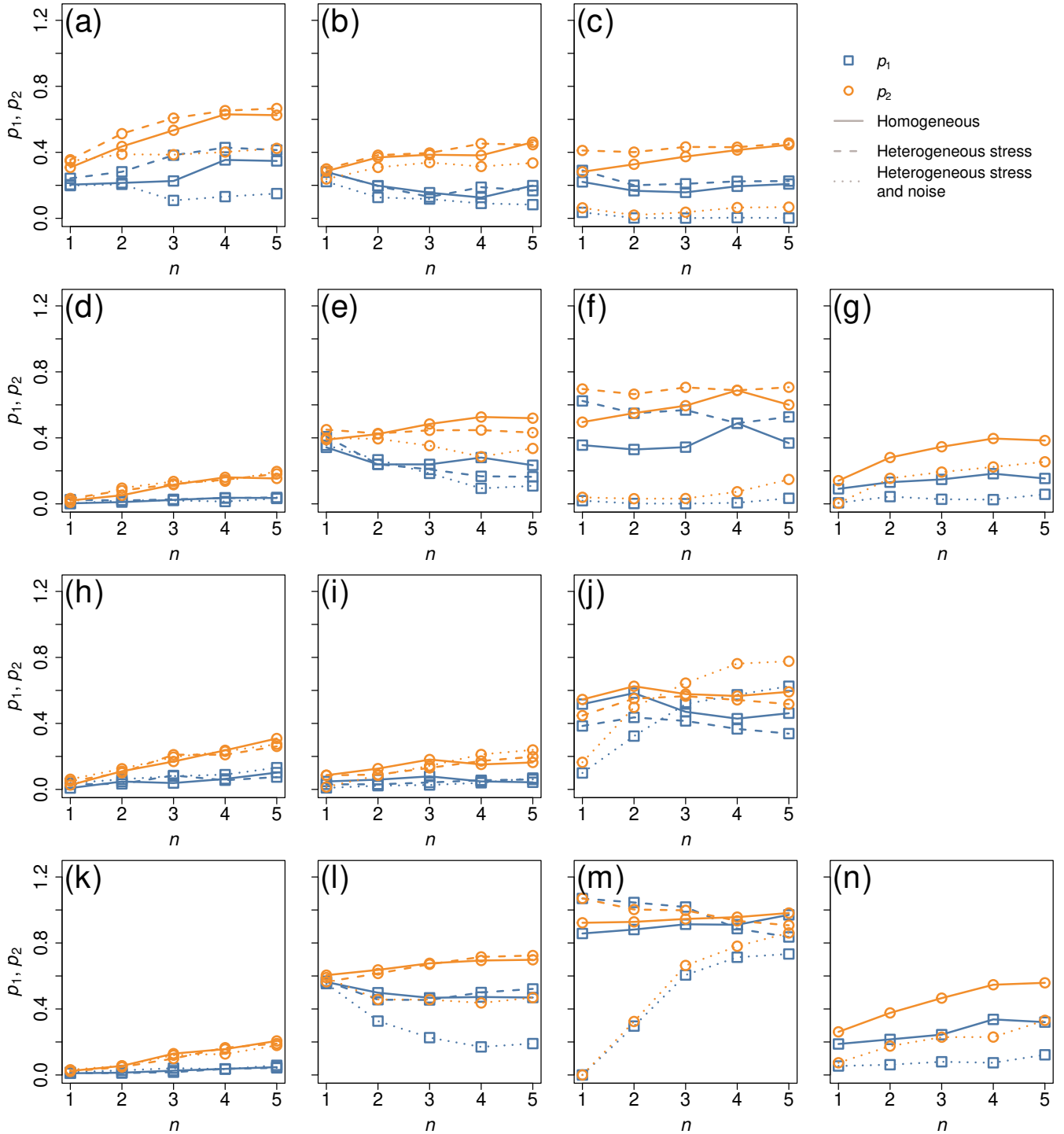


**Figure 8.** Performance of the node set maximizing  $d$  on the BA and Chesapeake Bay networks. The squares and circles represent  $p_1$  and  $p_2$ , respectively, for the given  $n$ , dynamics, network, and condition (i.e., whether  $u_i$  or  $\sigma_i$  is homogeneously or heterogeneously distributed) averaged over 50 series of simulations. (a)–(g): BA network. (h)–(n): Chesapeake Bay carbon flow network. The panels on the leftmost column correspond to the double-well dynamics, and the second to the fourth columns to the mutualistic interaction, gene regulatory, and SIS dynamics, respectively. The combination of the dynamics model and bifurcation parameter is as follows. (a) and (h): double-well,  $u$ . (b) and (i): mutualistic interaction,  $u$ . (c) and (j): gene regulatory,  $u$ . (d) and (k): double-well,  $D$ . (e) and (l): mutualistic interaction,  $D$ . (f) and (m): gene regulatory,  $D$ . (g) and (n): SIS,  $\lambda$ .

parameters (i.e.,  $u$  or  $D$ ), we have found that the result that  $p_1$  and  $p_2$  are small in most cases is robust. Specifically,  $p_1$  and  $p_2$  are considerably smaller than 1 when they are so for the original pairs of the bifurcation parameter value, the two bifurcation parameter values are not too close to each other, and the larger bifurcation parameter value is reasonably close to the first tipping point. (See Supplementary Note 2 for the numerical results.)

Not all the regime shifts accompany critical slowing down. Early warning signals based on critical slowing down, including  $\hat{V}_S$  for any node set  $S$ , should be insensitive to such types of regime shifts<sup>1,11,14,48</sup>. To verify that this is the case, we investigated coupled double-well dynamics on the BA network experiencing a state transition from the lower to the upper state of  $x_i(t)$  driven by either dynamical noise or impulse input given to  $x_i(t)$ 's. Dynamical noise and impulse input are two major scenarios in which regime shifts occur without critical slowing down<sup>11,14</sup>. It should be noted that, in both scenarios, all the system parameter values remain the same throughout a simulation. As expected,  $\hat{V}_S$  is found to be insensitive to impending regime shifts until they are about to occur, and therefore,  $\tau$  is close to 0. These results hold true for any choice of  $S$ , and the  $S$  maximizing  $d$  does not yield a particularly large  $\tau$  value. See Supplementary Note 7 for details.

In contrast to the last case, critical slowing down can occur even when there is no sudden regime shift. Representative examples of this phenomenon are transcritical and Hopf bifurcations<sup>14,49</sup>. The gene regulatory and SIS models that we have employed show transcritical bifurcations, at least in well-mixed populations. We showed that  $\hat{V}_S$  increases just before the bifurcation, which is captured by large  $\tau$  values, in the gene regulatory and SIS models (see Supplementary Note 8 for numerical evidence). Therefore, consistent with the previous studies<sup>14,49</sup>, we are not claiming that  $\hat{V}_S$  specifically increases when a bifurcation accompanying a large regime shift, which is typically a saddle-node bifurcation, is being approached.

Last, we derived theory for the variance of  $x_i(t)$  and its average over nodes for mathematical convenience. However, the standard deviation of  $x_i(t)$  rather than the variance of  $x_i(t)$  is also a common early warning signal for anticipating tipping points<sup>13,50,51</sup>. We verified that the results on the advantage of the maximizer of  $d$  remained almost the same when we used the average of the sample standard deviation of  $x_i(t)$  over  $i \in S$  as the early warning signal (see Supplementary Note 9).

### Comparison with other node selection methods

A simple heuristic to select a node set for constructing early warning signals by averaging is to use the  $n$  nodes with the largest standard deviation of  $x_i$ <sup>29</sup>, which we refer to as "Large SD". While there are also other strategies to select node sets, here we compare ours with Large SD because the measurement of the standard deviation of  $x_i$  does not require the information about the network structure, and therefore it is fair to compare Large SD and the present method. The crosses in Fig. 6 indicate the Kendall's  $\tau$  value for the double-well dynamics on the BA network when we use the  $n$  nodes with the largest standard deviation to calculate the early warning signal. Large SD detects the best single node, which the maximization of  $d$  does not (see Fig. 6(a)), Large SD also outperforms the maximizer of  $d$ , yielding larger  $\tau$  values, when  $n \in \{2, 3, 4, 5\}$  (see Figs. 6(b)–(e)), whereas the advantage of Large SD is marginal for  $n = 5$ . Therefore, when  $u_i$  and  $\sigma_i$  are homogeneous, Large SD beats the maximizer of  $d$ , at least for this example. However, the maximizer of  $d$  usually behaves much better than Large SD when  $\sigma_i$  is heterogeneous. Figure 9 shows an example. In this figure, we used the double-well dynamics on the BA network, as we did for Fig. 6, and assumed that both  $u_i$  and  $\sigma_i$  are heterogeneous. The figure indicates that the maximizer of  $d$  substantially outperforms Large SD except when  $n = 4$  and  $n = 5$ , for which the maximizer of  $d$  only slightly outperforms Large SD. The compromised performance of Large SD in this scenario is because Large SD tends to select nodes with large  $\sigma_i$  although a large  $\sigma_i$  value simply reflects that the  $i$ th node is inherently noisier than others.

To compare between the maximizer of  $d$  and Large SD more systematically, we compared the Kendall's  $\tau$  values attained by these two strategies for the six networks, the four dynamics models, and whether the stress or dynamical noise is homogeneous or heterogeneous across the nodes. As we show in Supplementary Note 8, we confirmed that the maximizer of  $d$  outperforms Large SD in a majority of cases when both the stress,  $u_i$ , and the noise strength,  $\sigma_i$ , are node-dependent. The maximizer of  $d$  outperforms Large SD even when  $\sigma_i$  is node-independent for the mutualistic interaction dynamics and  $D$  being used as the bifurcation parameter. In the other cases, the maximizer of  $d$  is either on par with or slightly inferior to Large SD. However, there is no case in which Large SD substantially outperforms the maximizer of  $d$  (i.e., Large SD outperforms the maximizer of  $d$  in terms of  $\tau$  by at most  $\approx 0.078$ ), whereas the maximizer of  $d$  often substantially outperforms Large SD.

Furthermore, we compared the maximizer of  $d$  with another heuristic algorithm with which one selects the  $n$  nodes that receive the highest total input (or lowest total input, depending on the direction of the bifurcation being considered) from the other nodes near the bifurcation point<sup>29</sup>, which we refer to as High/Low Input. The results of comparison between the maximizer of  $d$  and High/Low Input were similar to the case of the comparison between the maximizer of  $d$  and Large LD (see Supplementary Note 10 for the methods and results). In other words, the maximizer of  $d$  tends to be better than the High/Low Input algorithm, in particular when the nodes' dynamics are assumed to be heterogeneous. We note that High/Low Input requires the adjacency matrix of the network, i.e., complete information on the network structure, which neither the maximizer of  $d$  nor Large SD requires.

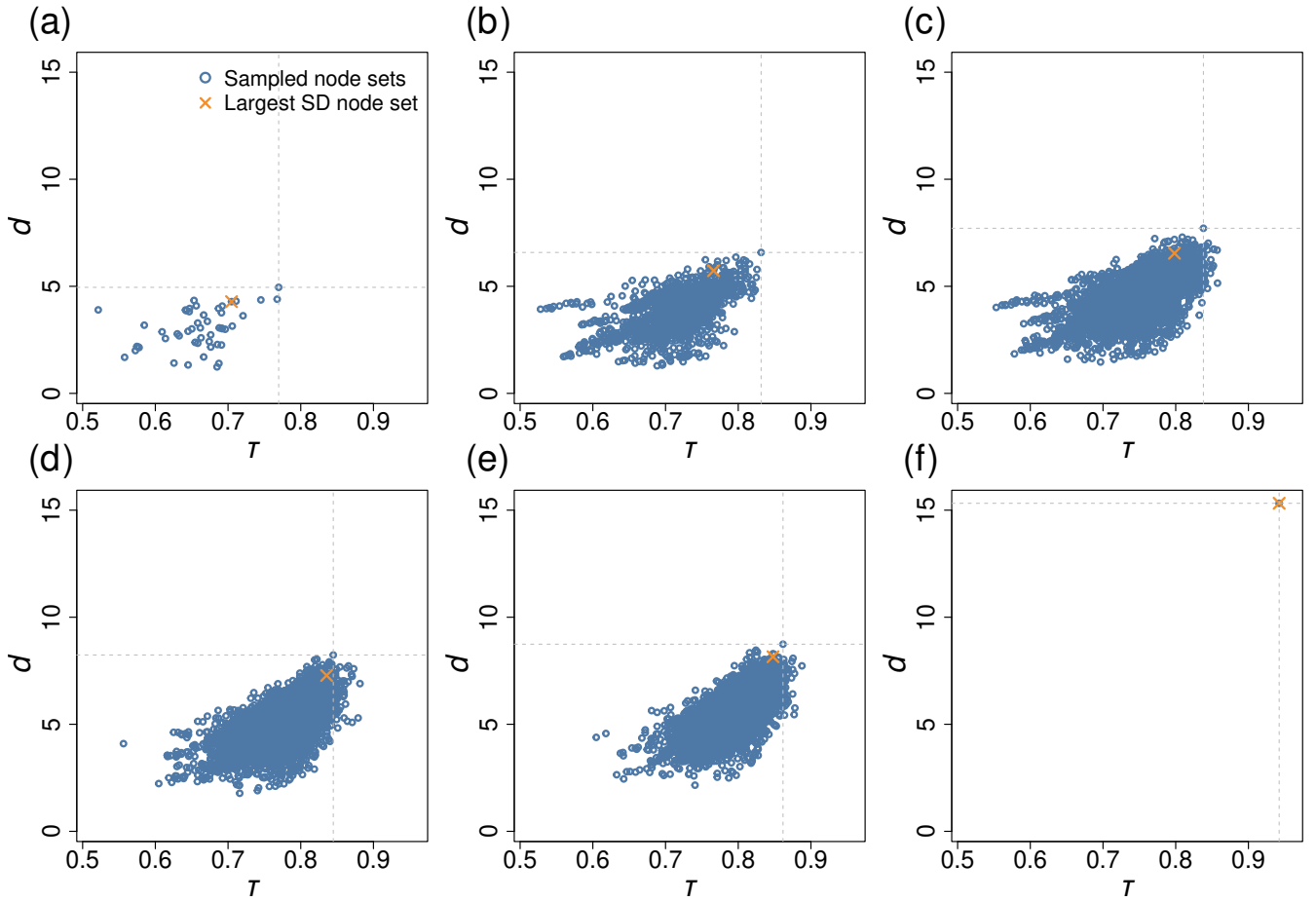


**Figure 9.** Relationships between the Kendall's  $\tau$  and  $d$  in the coupled double-well dynamics on the BA network with  $N = 50$  nodes under heterogeneous node stress and heterogeneous dynamical noise. The network is the same as the one used in Fig. 6. We considered node sets  $S$  with  $n \in \{1, 2, 3, 4, 5, N\}$  nodes. (a)  $n = 1$ . (b)  $n = 2$ . (c)  $n = 3$ . (d)  $n = 4$ . (e)  $n = 5$ . (f)  $n = N$ . The  $\tau$  and  $d$  values for the node set maximizing  $d$  are highlighted by the dashed lines. The cross represents ‘‘Large SD’’, i.e., the node set comprised of the  $n$  nodes with the largest sample standard deviation of  $x_i(t)$ .

## 412 Discussion

413 Based on theory of OU processes, we proposed an objective function  $d$  for identifying sets of nodes,  $S$ , that are expected to  
414 reliably alert impending tipping events when we combine the early warning signals from  $S$  by averaging. While we focused on  
415 anticipating the first bifurcation in the entire network, the proposed method is equally applicable to anticipating the second and  
416 later transitions in the case of multistage transitions in which different nodes experience regime shifts at different timings<sup>11,25–29</sup>.  
417 We numerically demonstrated the proposed method with various dynamics models, networks, and system heterogeneity  
418 scenarios to confirm its good performances. Application to domain-specific problems such as in ecology, climate dynamics,  
419 and disease progression is saved for future work. In these and other applications, further complexity of systems in question  
420 in addition to the network structure and nonlinearity that we have neglected, such as the mixture of positive and negative  
421 interactions<sup>18</sup> and nonequilibrium dynamics<sup>32</sup>, may require alternations of our method, posing further research questions.

422 Nonetheless, our method is readily applicable to empirical data because it does not require the information about the  
423 network structure or the dynamical model equations. It only requires the covariance matrix among the observables measured  
424 at two values of the bifurcation parameter, or two different states of the networked system, to determine an optimal sentinel  
425 node set,  $S$ . In ecological<sup>52,53</sup> and psychopathological<sup>54</sup> applications of early warning signals, it is customary to calculate  
426 fluctuation-based early warning signals such as the variance or covariance from multivariate time series data with sliding time  
427 windows, thus obtain time series of early warning signals, and use them to give alerts for impending tipping points. To apply  
428 our methods to empirical multivariate time series data, once one has determined  $S$  as the maximizer of  $d$ , one only needs to  
429 collect signals from the nodes in  $S$  in each of the sliding time windows, calculate the early warning signal (i.e.,  $\hat{V}_S$ ), and monitor  
430 it.

431 The proposed method tended to outperform other heuristics when the amount of dynamical noise depended on nodes.  
432 The assumption of heterogeneous noise, also made in a previous analytical study<sup>24</sup>, is probably realistic because the nodes  
433 constituting a complex dynamical system correspond to different species or geographical patches in ecosystems, different genes  
434 or symptoms in complex systems of diseases, different firms or countries in a financial network, and so on. Although it is  
435 not easy to measure dynamical noise for each node in isolation in empirical complex systems, there is no a priori reason to  
436 assume that different nodes are subject to the same amount of intrinsic noise. As we have shown, heterogeneous noise across  
437 nodes generally confuses early warning signals estimated from observed data because, in heterogeneous noise cases, a larger  
438 variance of an  $x_i$  does not imply that  $x_i$  provides a better early warning signal. We overcame this problem by quantifying  
439 fluctuations of the early warning signal, not just fluctuations of  $x_i$ , and measuring it at two bifurcation parameter values. We  
440 propose that we should observe the system at two sufficiently distant bifurcation parameter values (practically, two distant  
441 times) for identifying good early warning signals. The early warning signals at nodes whose fluctuation is large due to large  
442 intrinsic noise do not substantially grow between the two bifurcation parameter values. In contrast, the early warning signals at  
443 nodes closely approaching their tipping point substantially grow between the two bifurcation parameter values. An alternative  
444 strategy is to use lagged autocorrelation as early warning signal because nodes with large intrinsic noise may produce small  
445 autocorrelation. Autocorrelation of multivariate OU processes is analytically tractable, whereas it is more complicated than the  
446 variance and covariance<sup>37</sup>. Analysis of autocorrelation and its average over nodes as early warning signals with the present  
447 theoretical framework warrants future work.

448 In numerical simulations, we examined the size of the node set  $n \in \{1, \dots, 5\}$ . For  $n = 1$  and 2, we inspected all the  
449 node sets for their performance and  $d$  values. In contrast, we randomly sampled node sets for  $n \geq 3$  due to the combinatorial  
450 explosion. If the number of nodes,  $N$ , is less than approximately 20, it may be feasible to exhaustively investigate all the node  
451 sets across all values of  $n$  to find the exact maximizer of  $d$ . Note that the calculation of a single  $d$  only involves the square and  
452 summation of the entry of the  $N \times N$  covariance matrix and therefore is not costly. When  $N$  is larger, we need to find node  
453 sets that only approximately maximize  $d$ . This combinatorial problem has scarcely been discussed in early warning signal  
454 research community. It is because prior studies highlighting that different nodes can emit early warning signals of different  
455 quality either used systems with a small number of nodes, typically with  $N \leq 5$ <sup>19,21–24</sup> or linearly ranked the  $N$  nodes<sup>20,27,29</sup>,  
456 thus implicitly abandoning the potential benefit of wisely combining different nodes. However, real-world complex systems  
457 whose tipping events are of practical interest are more often than not larger complex networks<sup>17,18</sup>. Although we provided a  
458 stopping criterion for exploring different  $n$  values and showed a demonstration (see Supplementary Note 4), further deploying  
459 heuristics for combinatorial optimization to approximate maximization of  $d$  for reasonably large  $n$  and  $N$  is left for future work.

460 We used the sample covariance matrix as the estimator of the true covariance matrix for simplicity. In fact, although the  
461 sample covariance matrix is an unbiased estimator in the limit of  $L \rightarrow \infty$ , it is an unreliable estimator when  $L$  is small relative to  
462  $N$ , and there are better choices such as different sparse estimators and covariance shrinkage methods<sup>45</sup>. In the present study, the  
463 sample covariance matrix is not problematic because we used a relatively small  $N$  and large  $L$ . However, in practical situations,  
464 we may only have a small number of samples, in which case one should consider a different covariance estimator. Furthermore,  
465 we confined ourselves to linear combinations of early warning signals measured at single nodes. However, a natural extension  
466 is to exploit covariance of  $x_i$  and  $x_j$ , where  $i \neq j$ , to construct early warning signals. Examples of such early warning signals

467 include the leading eigenvalue of the covariance matrix<sup>21,55,56</sup> and Moran's  $I$ <sup>57–59</sup>. It should be noted that we used the cross  
 468 covariance,  $C_{ij}^{(1)}$  and  $C_{ij}^{(2)}$ , where  $i \neq j$ , only to evaluate the uncertainty of our early warning signals, not to construct early  
 469 warning signals. Early warning signals for heterogeneous networks when the number of samples is limited are a challenging  
 470 open question.

## 471 Methods

### 472 Dynamical system models

473 We used the following four types of dynamics on networks with dynamical noise.

474 A coupled double-well model on networks with dynamical noise is given by Eq. (26). We set  $(r_1, r_2, r_3) = (1, 3, 5)$ . In  
 475 the presence of coupling (i.e.,  $D > 0$ ), the lower and the upper state of each node is around  $x_i = r_1$  and  $x_i = r_3$ , respectively.  
 476 Here we succinctly regard that the nodes with  $x_i < r_2$  and  $x_i \geq r_2$  are in the lower and the upper state, respectively. We set  
 477  $u_i = u + \Delta u_i \forall i$ . If  $u$  is the bifurcation parameter, we initially set  $u = 0$  and  $D = 0.05$ . If  $D$  is the bifurcation parameter, we  
 478 initially set  $u = 0$  and  $D = 0$ . In the case of homogeneous stress, we set  $\Delta u_i = 0 \forall i$ . In the case of heterogeneous stress, we  
 479 draw each  $\Delta u_i$  independently from the uniform density on  $[-0.25, 0.25]$  for this and the following three models of dynamics.  
 480 We set  $\sigma_i = \sigma + \Delta \sigma_i$ , where  $\sigma = 0.05$  for this model. We set  $\Delta \sigma_i = 0 \forall i$  in the homogeneous noise case and draw  $\Delta \sigma_i$  from  
 481 the uniform density on  $[-0.9\sigma, 0.9\sigma]$  in the heterogeneous noise case, including for the other three dynamical system models  
 482 described in the remainder of this section.

483 The mutualistic interaction dynamics among species is given by

$$484 \mathrm{d}x_i = \left[ B_i + x_i \left( 1 - \frac{x_i}{K_i} \right) \left( \frac{x_i}{C_i} - 1 \right) + D \sum_{j=1}^N w_{ij} \frac{x_i x_j}{\tilde{D}_i + E_i x_i + H_j x_j} \right] \mathrm{d}t + \sigma_i \mathrm{d}W_i, \quad (27)$$

485 where  $x_i$  represents the abundance of the  $i$ th species, and  $B_i$ ,  $C_i$ ,  $\tilde{D}_i$ ,  $E_i$ ,  $H_i$ , and  $K_i$  (with  $i \in \{1, \dots, N\}$ ) are constants<sup>46</sup>. Constant  
 486  $B_i$  represents the migration rate of the  $i$ th species from outside the entire ecosystem. The second term on the right-hand side of  
 487 Eq. (27) represents the logistic growth with carrying capacity  $K_i$  and Allee constant  $C_i$ . The third term represents the mutualistic  
 488 effect of the  $j$ th species on the  $i$ th species under the assumption that  $w_{ij} \geq 0$ . This term is bounded by definition for preventing  
 489  $x_i$  to exceed  $K_i$  to break down the logistic growth nature of the second term. We set  $B_i = 0.1 + u + \Delta u_i$ ,  $C_i = 1$ ,  $\tilde{D}_i = 5$ ,  $E_i = 0.9$ ,  
 490  $H_i = 0.1$ , and  $K_i = 5 \forall i \in \{1, \dots, N\}$ , following Ref.<sup>46</sup>. Regardless of whether  $u$  or  $D$  is the bifurcation parameter, we initially  
 491 set  $u = 0$  and  $D = 1$ . We confirmed that all  $x_i$  were in their upper state (i.e.,  $\gg 0$ ) at equilibrium when  $(u, D) = (0, 1)$ . We set  
 492  $\sigma_i = \sigma + \Delta \sigma_i$  with  $\sigma = 0.25$ .

493 The gene regulatory dynamics is given by

$$494 \mathrm{d}x_i = \left( -B x_i^f + D \sum_{j=1}^N w_{ij} \frac{x_j^h}{x_j^h + 1} + u_i \right) \mathrm{d}t + \sigma_i \mathrm{d}W_i, \quad (28)$$

495 where  $x_i$  represents the expression level of the  $i$ th gene<sup>46</sup>. We set  $B = 1$ ,  $f = 1$ , and  $h = 2$  by following Ref.<sup>46</sup>, and also  
 496  $u_i = u + \Delta u_i$ . Regardless of whether  $u$  or  $D$  is the bifurcation parameter, we initially set  $u = 0$  and  $D = 1$ . Then, we obtain  
 497  $x_i > 0.1 \forall i$  at equilibrium if the initial values of  $x_i \forall i$  are sufficiently large, which we assume. We set  $\sigma_i = \sigma + \Delta \sigma_i$ , where  
 498  $\sigma = 5 \times 10^{-6}$ .

499 The SIS dynamics on networks with dynamical noise is given by

$$500 \mathrm{d}x_i = \left( \lambda \sum_{j=1}^N w_{ij} (1 - x_j) x_j - \mu x_i \right) \mathrm{d}t + \sigma_i \mathrm{d}W_i, \quad (29)$$

501 where  $x_i$  represents the probability that the  $i$ th node is infectious,  $\lambda$  is the infection rate (specifically, the rate at which the  $i$ th  
 502 node is infected by an infectious neighbor) and is equivalent to  $D$  in the coupled double-well, mutualistic interaction, and  
 503 gene regulatory dynamics models, and  $\mu$  is the recovery rate. The first term on the right-hand side of Eq. (29) represents  
 504 that the  $j$ th node infects the  $i$ th node. The second term represents the recovery of the  $i$ th node. We set  $\mu = 1$  without loss of  
 505 generality; multiplying  $\lambda$ ,  $\mu$ , and  $\sigma_i$  by the same positive constant is equivalent to changing the time scale and not to change  
 506 these parameter values. For this model, we only use  $\lambda$  as the bifurcation parameter. This is because adding a term  $u_i \mathrm{d}t$  on the  
 507 right-hand side of Eq. (29) would imply that infectious individuals can spontaneously appear in the population in the absence  
 508 of any infected host, which is unrealistic. For the same reason, we do not have a concept of heterogeneous node stress in  
 509 this model. We initially set  $\lambda = 0$ . In the absence of dynamical noise, it holds true that  $0 \leq x_i < 1 \forall i$  at equilibrium. We set  
 510  $\sigma_i = \sigma + \Delta \sigma_i$ , where  $\sigma = 5 \times 10^{-4}$ .

## 505 Networks

506 We used the following three model networks and three empirical networks in our numerical simulations. All networks are  
 507 undirected and unweighted by construction, or coerced to be so.

508 The first network was generated by the Erdős-Rényi random graph with 50 nodes and exactly 125 edges. We connected a  
 509 uniformly randomly selected pair of nodes that had not yet been adjacent to each other, one by one, until we had 125 edges. It  
 510 happened that the generated network was connected. By construction, the average degree  $\langle k \rangle = 5$ .

511 The second network is a network generated by the BA model with  $N = 50$  nodes. We set the number of edges per each  
 512 additional node to  $m = 2$ . The initial condition was the complete graph with 3 nodes (i.e., triangle). In the limit  $N \rightarrow \infty$ , the  
 513 model produces a degree distribution with a power-law tail, i.e.,  $p(k) \propto k^{-3}$ , where  $k$  is the degree, and  $p(k)$  is the probability  
 514 that the degree is equal to  $k$ . The resulting network was connected and had 97 edges, yielding  $\langle k \rangle = 3.88$ .

515 The third network is the largest connected component of the node fitness model proposed by Goh et al. <sup>60–62</sup>. This model  
 516 produces networks with heterogeneous degree distributions as follows. We start with an empty network with  $N = 50$  nodes and  
 517 assign to each node  $i$  a fitness score  $f_i = (i + i_0 - 1)^{-\alpha}$ , where  $\alpha$  is a parameter that controls the heterogeneity of the degree  
 518 distribution, and  $i_0 = N^{1-\frac{1}{\alpha}} \left[ 10\sqrt{2}(1-\alpha) \right]^{\frac{1}{\alpha}}$  constrains the maximum degree. We set  $\alpha = 2$ . Then, we independently connect  
 519 each pair of nodes  $(i, j)$  by an edge with probability  $f_i f_j / (\sum_{\ell=1}^N f_\ell)^2$ . We took the largest connected component of the resulting  
 520 network, which included  $N = 49$  nodes and 125 edges, yielding  $\langle k \rangle = 5.1$ .

521 The fourth network is a record of carbon flows in the Chesapeake Bay marine ecosystem<sup>63</sup>. The original carbon flow data is  
 522 directed and forms a connected network. We used the undirected, unweighted version of the network stored by the Koblenz  
 523 Network Collection<sup>64</sup>. This network has 39 nodes, 170 edges, and  $\langle k \rangle = 8.72$ .

524 The fifth network is the food web of a freshwater stream collected in southern New Zealand<sup>65</sup>. Two species are connected if  
 525 there was evidence of one consuming the other. The original data is a directed and unweighted network with 49 nodes and 110  
 526 edges<sup>66</sup>. We coerced the network to be undirected and retained the largest connected component, resulting in a network with 48  
 527 nodes, 110 edges, and  $\langle k \rangle = 4.58$ .

528 The sixth network is a social network of wild dolphins observed in Doubtful Sound, New Zealand<sup>67</sup>. The network is  
 529 connected, undirected, and unweighted, with 62 nodes, 159 edges, and  $\langle k \rangle = 5.13$ .

## 530 Calculation and performance assessment of early warning signals

531 We conducted 50 independent series of simulations for each combination of dynamics model, network, and whether both node  
 532 stress (i.e.,  $u_i$ ) and noise strength (i.e.,  $\sigma_i$ ) were homogeneous, only  $u_i$  was heterogeneous, or both  $u_i$  and  $\sigma_i$  were heterogeneous.  
 533 Each series consisted of simulations at linearly increasing values of a bifurcation parameter in the case of the double-well or SIS  
 534 dynamics, and linearly decreasing values of a bifurcation parameter in the case of the mutualistic interaction or gene regulatory  
 535 dynamics. When we moved to a next value of the bifurcation parameter, we increased it by  $\Delta u = 0.025$  or  $\Delta D = 0.0025$  for  
 536 the double-well dynamics, decreased it by  $\Delta u = 0.1$  or  $\Delta D = 0.01$  for the mutualistic interaction dynamics, decreased it by  
 537  $\Delta u = 0.01$  or  $\Delta D = 0.01$  for the gene regulatory dynamics, and increased it by  $\Delta \lambda = 0.0025$  for the SIS dynamics.

538 Each simulation given the dynamics model began from the same value of  $x_i \forall i$  (double-well:  $x_i = 1$ , mutualistic interaction:  
 539  $x_i = 5$ , gene regulatory:  $x_i = 5$ , SIS:  $x_i = 0.001$ ) regardless of the bifurcation parameter value. We used the Euler-Maruyama  
 540 method with  $\Delta t = 0.01$  to simulate each dynamics. In the SIS and gene regulatory dynamics, whenever we obtain a negative  
 541 value of  $x_i(t)$  for any  $i$  due to dynamical noise, we reset  $x_i(t) = 0$ . We allowed 100 generic time units (TU) to discard transients,  
 542 except in the case of the mutualistic dynamics, for which we allowed 10 TU due to a shorter characteristic time scale of the  
 543 mutualistic dynamics model. After discarding transients, we considered the system at equilibrium and took  $L = 100$  evenly  
 544 spaced samples from each  $x_i(t)$ ,  $i \in \{1, 2, \dots, N\}$ ; samples were spaced 1 TU apart, with the exception of the mutualistic  
 545 dynamics model for which the samples were spaced 0.1 TU apart. We stopped a series of simulations with a gradually  
 546 changing bifurcation parameter value once any  $x_i$  was no longer near its initial state, specifically, once any  $x_i$  satisfies the  
 547 following condition:  $x_i \geq 3$  for the double-well dynamics,  $x_i < 0.1$  for the mutualistic interaction dynamics,  $x_i < 0.1$  for the  
 548 gene regulatory dynamics, and  $x_i \geq 0.1$  for the SIS dynamics.

549 After all simulations in a given series were complete, we calculated the early warning signals for each node set  $S$   
 550 with  $|S| = n$ , based on the  $L$  samples taken at each value of the bifurcation parameter. In addition, to calculate  $d$ , we  
 551 used Eq. (5) to obtain  $\mu_1 = \frac{1}{n} \sum_{i=1}^n C_{ii}^{(1)}$  and  $\mu_2 = \frac{1}{n} \sum_{i=1}^n C_{ii}^{(2)}$ , and Eq. (6) to obtain  $\text{var}_1 = \frac{2}{n^2(L-1)} \sum_{i=1}^n \sum_{j=1}^n (C_{ij}^{(1)})^2$  and  
 552  $\text{var}_2 = \frac{2}{n^2(L-1)} \sum_{i=1}^n \sum_{j=1}^n (C_{ij}^{(2)})^2$ . Then, we used Eq. (15) to calculate  $d$  for the node set  $S$ . Note that this computation is easy  
 553 once we have calculated  $C^{(1)}$  and  $C^{(2)}$ . We selected the two values of the bifurcation parameter at which we calculated  $C^{(1)}$  and  
 554  $C^{(2)}$  as follows. Suppose that the bifurcation parameter is  $u$  and that we have simulated the dynamics at  $u = \bar{u}_k$ ,  $k \in \{1, 2, \dots, \tilde{K}\}$ .  
 555 Thus, the simulation with  $\bar{u}_{\tilde{K}}$  was the last simulation in which all  $x_i$  remained near their initial state at equilibrium. We selected  
 556  $k^{(1)} = \text{round}(0.1\tilde{K})$  and  $k^{(2)} = \text{round}(0.9\tilde{K})$ , where  $\text{round}()$  denotes rounding to the closest integer. Then, we calculated  $C^{(1)}$

557 and  $C^{(2)}$  from the  $L$  samples obtained at  $u = u^{(1)} \equiv \bar{u}_{k^{(1)}}$  and  $u = u^{(2)} \equiv \bar{u}_{k^{(2)}}$ , respectively. We followed the same procedure to  
558 select the two values of  $D$  at which we calculated  $C^{(1)}$  and  $C^{(2)}$  when the bifurcation parameter was  $D$ .

559 In addition to by maximizing  $d$ , we also determined node set  $S$  by the Large SD algorithm<sup>29</sup> for comparison purposes,  
560 which proceeds as follows. First, we collected  $L$  samples from each  $x_i(t)$  at  $u = u^{(2)}$  (or  $D = D^{(2)}$  when  $D$  instead of  $u$  was the  
561 bifurcation parameter) and calculated its sample standard deviation. Second, we defined  $S$  as the set of the  $n$  nodes with the  
562 largest sample standard deviation of  $x_i(t)$ . Third, we averaged the sample standard deviation of  $x_i(t)$  over  $i \in S$  and used it as  
563 early warning signal.

564 We quantify the extent to which a given node set  $S$  signals the proximity of tipping by the Kendall's  $\tau$  rank correlation  
565 between the early warning signal (i.e., the sample variance averaged over the nodes in  $S$  unless we state otherwise) and the  
566 bifurcation parameter<sup>13</sup>. Because of critical slowing down, the variance of  $x_i(t)$  grows large as the dynamical system approaches  
567 a tipping point<sup>1</sup>. In our simulations, when the bifurcation parameter linearly increases (i.e., double-well and SIS dynamics),  
568 the value of a perfect early warning signal would monotonically increase, resulting in  $\tau = 1$ . When the bifurcation parameter  
569 linearly decreases (i.e., mutualistic interaction and gene regulatory dynamics), a perfect early warning signal yields  $\tau = -1$ .

## 570 **Data availability**

571 The numerical data that are generated during the current study and underlie the figures in this article are available on Github at  
572 <https://github.com/ngmaclaren/mixing-EWS>.

## 573 **Code availability**

574 The code for generating the results and figures in this article is publicly available on Github at <https://github.com/ngma->  
575 [claren/mixing-EWS](https://github.com/ngmaclaren/mixing-EWS).

## 576 **References**

- 577 1. Scheffer, M. *et al.* Early-warning signals for critical transitions. *Nature* **461**, 53–59 (2009).
- 578 2. Scheffer, M., Carpenter, S. R., Dakos, V. & Van Nes, E. H. Generic indicators of ecological resilience: Inferring the chance  
579 of a critical transition. *Annu. Rev. Ecol. Evol. Syst.* **46**, 145–167 (2015).
- 580 3. Liu, Y., Kumar, M., Katul, G. G. & Porporato, A. Reduced resilience as an early warning signal of forest mortality. *Nat. Clim. Chang.* **9**, 880–885 (2019).
- 581 4. Wunderling, N. *et al.* Recurrent droughts increase risk of cascading tipping events by outpacing adaptive capacities in the  
582 Amazon rainforest. *Proc. Natl. Acad. Sci. USA* **119**, e2120777119 (2022).
- 583 5. Southall, E., Brett, T. S., Tildesley, M. J. & Dyson, L. Early warning signals of infectious disease transitions: A review. *J. R. Soc. Interface* **18**, 20210555 (2021).
- 584 6. van de Leemput, I. A. *et al.* Critical slowing down as early warning for the onset and termination of depression. *Proc. Natl. Acad. Sci. USA* **111**, 87–92 (2014).
- 585 7. Helmich, M. A. *et al.* Early warning signals and critical transitions in psychopathology: Challenges and recommendations. *Curr. Opin. Psychol.* **41**, 51–58 (2021).
- 586 8. Dablander, F., Pichler, A., Cika, A. & Bacilieri, A. Anticipating critical transitions in psychological systems using early  
587 warning signals: Theoretical and practical considerations. *Psychol. Methods* **Ahead of print**, 1–26 (2022).
- 588 9. Liu, X. *et al.* Detection for disease tipping points by landscape dynamic network biomarkers. *Nat. Sci. Rev.* **6**, 775–785  
589 (2019).
- 590 10. Aihara, K., Liu, R., Koizumi, K., Liu, X. & Chen, L. Dynamical network biomarkers: Theory and applications. *Gene* **808**,  
591 145997 (2022).
- 592 11. Scheffer, M. *et al.* Anticipating critical transitions. *Science* **338**, 344–348 (2012).
- 593 12. Boettiger, C. & Hastings, A. Early warning signals and the prosecutor's fallacy. *Proc. R. Soc. B* **279**, 4734–4739 (2012).
- 594 13. Dakos, V. *et al.* Methods for detecting early warnings of critical transitions in time series illustrated using simulated  
595 ecological data. *PLoS ONE* **7**, e41010 (2012).
- 596 14. Boettiger, C., Ross, N. & Hastings, A. Early warning signals: The charted and uncharted territories. *Theor. Ecol.* **6**,  
597 255–264 (2013).

602 15. Dakos, V., Carpenter, S. R., van Nes, E. H. & Scheffer, M. Resilience indicators: Prospects and limitations for early  
603 warnings of regime shifts. *Phil. Trans. R. Soc. B* **370**, 20130263 (2015).

604 16. Liu, X. *et al.* Network resilience. *Phys. Rep.* **971**, 1–108 (2022).

605 17. Scheffer, M. *et al.* Quantifying resilience of humans and other animals. *Proc. Natl. Acad. Sci. USA* **115**, 11883–11890  
606 (2018).

607 18. Kéfi, S., Saade, C., Berlow, E. L., Cabral, J. S. & Fronhofer, E. A. Scaling up our understanding of tipping points. *Phil.*  
608 *Trans. R. Soc. B* **377**, 20210386 (2022).

609 19. Boerlijst, M. C., Oudman, T. & de Roos, A. M. Catastrophic collapse can occur without early warning: Examples of silent  
610 catastrophes in structured ecological models. *PLoS ONE* **8**, e62033 (2013).

611 20. Dakos, V. & Bascompte, J. Critical slowing down as early warning for the onset of collapse in mutualistic communities.  
612 *Proc. Natl. Acad. Sci. USA* **111**, 17546–17551 (2014).

613 21. Dakos, V. Identifying best-indicator species for abrupt transitions in multispecies communities. *Ecol. Ind.* **94**, 494–502  
614 (2018).

615 22. Weinans, E. *et al.* Finding the direction of lowest resilience in multivariate complex systems. *J. R. Soc. Interface* **16**,  
616 20190629 (2019).

617 23. Ghadami, A., Chen, S. & Epureanu, B. I. Data-driven identification of reliable sensor species to predict regime shifts in  
618 ecological networks. *R. Soc. Open Sci.* **7**, 200896 (2020).

619 24. Patterson, A. C., Strang, A. G. & Abbott, K. C. When and where we can expect to see early warning signals in multispecies  
620 systems approaching tipping points: Insights from theory. *Am. Nat.* **198**, E12–E26 (2021).

621 25. Lever, J. J. *et al.* Foreseeing the future of mutualistic communities beyond collapse. *Ecol. Lett.* **23**, 2–15 (2020).

622 26. Wunderling, N., Gelbrecht, M., Winkelmann, R., Kurths, J. & Donges, J. F. Basin stability and limit cycles in a conceptual  
623 model for climate tipping cascades. *New J. Phys.* **22**, 123031 (2020).

624 27. Aparicio, A., Velasco-Hernández, J. X., Moog, C. H., Liu, Y.-Y. & Angulo, M. T. Structure-based identification of sensor  
625 species for anticipating critical transitions. *Proc. Natl. Acad. Sci. USA* **118**, e2104732118 (2021).

626 28. Kundu, P., MacLaren, N. G., Kori, H. & Masuda, N. Mean-field theory for double-well systems on degree-heterogeneous  
627 networks. *Proc. R. Soc. A* **478**, 20220350 (2022).

628 29. MacLaren, N. G., Kundu, P. & Masuda, N. Early warnings for multi-stage transitions in dynamics on networks. *J. R. Soc.*  
629 *Interface* **20**, 20220743 (2023).

630 30. Chen, L., Liu, R., Liu, Z.-P., Li, M. & Aihara, K. Detecting early-warning signals for sudden deterioration of complex  
631 diseases by dynamical network biomarkers. *Sci. Rep.* **2**, 342 (2012).

632 31. Vafaei, F. Using multi-objective optimization to identify dynamical network biomarkers as early-warning signals of  
633 complex diseases. *Sci. Rep.* **6**, 22023 (2016).

634 32. Medeiros, L. P., Allesina, S., Dakos, V., Sugihara, G. & Saavedra, S. Ranking species based on sensitivity to perturbations  
635 under non-equilibrium community dynamics. *Ecol. Lett.* **26**, 170–183 (2023).

636 33. Van Kampen, N. G. *Stochastic Processes in Physics and Chemistry* (Elsevier, Amsterdam, The Netherlands, 2007), third  
637 edn.

638 34. Pernice, V., Staude, B., Cardanobile, S. & Rotter, S. How structure determines correlations in neuronal networks. *PLoS*  
639 *Comput. Biol.* **7**, e1002059 (2011).

640 35. Kiss, I. Z., Miller, J. C. & Simon, P. L. *Mathematics of Epidemics on Networks* (Springer, Cham, Switzerland, 2017).

641 36. Koizumi, K. *et al.* Identifying pre-disease signals before metabolic syndrome in mice by dynamical network biomarkers.  
642 *Sci. Rep.* **9**, 8767 (2019).

643 37. Gardiner, C. *Stochastic Methods* (Springer-Verlag, Berlin, 2009), fourth edn.

644 38. Gajić, Z. & Qureshi, M. T. J. *Lyapunov Matrix Equation in System Stability and Control* (Academic Press, San Diego, CA,  
645 USA, 1995).

646 39. Carpenter, S. R. & Brock, W. A. Rising variance: A leading indicator of ecological transition. *Ecol. Lett.* **9**, 311–318  
647 (2006).

648 40. Harris, M. J., Hay, S. I. & Drake, J. M. Early warning signals of malaria resurgence in Kericho, Kenya. *Biol. Lett.* **16**,  
649 20190713 (2020).

650 41. Boers, N. Observation-based early-warning signals for a collapse of the Atlantic Meridional Overturning Circulation. *Nat. Clim. Chang.* **11**, 680–688 (2021).

651 42. Weinans, E., Quax, R., van Nes, E. H. & van de Leemput, I. A. Evaluating the performance of multivariate indicators of resilience loss. *Sci. Rep.* **11**, 9148 (2021).

652 43. Kuznetsov, Y. A. *Elements of Applied Bifurcation Theory* (Springer-Verlag, NY, USA, 1998), second edn.

653 44. Abou-Moustafa, K. T., De La Torre, F. & Ferrie, F. P. Designing a metric for the difference between Gaussian densities. In *Advances in Intelligent and Soft Computing*, vol. 83, 57–70 (Springer-Verlag, Berlin, Germany, 2010).

654 45. Bun, J., Bouchaud, J. P. & Potters, M. Cleaning large correlation matrices: Tools from Random Matrix Theory. *Phys. Rep.* **666**, 1–109 (2017).

655 46. Gao, J., Barzel, B. & Barabási, A. L. Universal resilience patterns in complex networks. *Nature* **530**, 307–312 (2016).

656 47. Pastor-Satorras, R., Castellano, C., Van Mieghem, P. & Vespignani, A. Epidemic processes in complex networks. *Rev. Mod. Phys.* **87**, 925–979 (2015).

657 48. Hastings, A. & Wysham, D. B. Regime shifts in ecological systems can occur with no warning. *Ecol. Lett.* **13**, 464–472 (2010).

658 49. Kéfi, S., Dakos, V., Scheffer, M., Van Nes, E. H. & Rietkerk, M. Early warning signals also precede non-catastrophic transitions. *Oikos* **122**, 641–648 (2013).

659 50. Boettner, C., Klinghammer, G., Boers, N., Westerhold, T. & Marwan, N. Early-warning signals for Cenozoic climate transitions. *Quat. Sci. Rev.* **270**, 107177 (2021).

660 51. O'Brien, D. A. & Clements, C. F. Early warning signal reliability varies with COVID-19 waves. *Biol. Lett.* **17**, 20210487 (2021).

661 52. Gsell, A. S. *et al.* Evaluating early-warning indicators of critical transitions in natural aquatic ecosystems. *Proc. Natl. Acad. Sci. USA* **113**, E8089–E8095 (2016).

662 53. Wilkinson, G. M. *et al.* Early warning signals precede cyanobacterial blooms in multiple whole-lake experiments. *Ecol. Monog.* **88**, 188–203 (2018).

663 54. Wichers, M., Groot, P. C., Psychosystems, E. & EWS Group. Critical slowing down as a personalized early warning signal for depression. *Psychother. Psychosom.* **85**, 114–116 (2016).

664 55. Brock, W. A. & Carpenter, S. R. Variance as a leading indicator of regime shift in ecosystem services. *Ecol. Soc.* **11**, 9 (2006).

665 56. Chen, S., O'Dea, E. B., Drake, J. M. & Epureanu, B. I. Eigenvalues of the covariance matrix as early warning signals for critical transitions in ecological systems. *Sci. Rep.* **9**, 2572 (2019).

666 57. Dakos, V., van Nes, E. H., Donangelo, R., Fort, H. & Scheffer, M. Spatial correlation as leading indicator of catastrophic shifts. *Theor. Ecol.* **3**, 163–174 (2010).

667 58. Kéfi, S. *et al.* Early warning signals of ecological transitions: Methods for spatial patterns. *PLoS ONE* **9**, e92097 (2014).

668 59. Jentsch, P. C., Anand, M. & Bauch, C. T. Spatial correlation as an early warning signal of regime shifts in a multiplex disease-behaviour network. *J. Theor. Biol.* **448**, 17–25 (2018).

669 60. Goh, K. I., Kahng, B. & Kim, D. Universal behavior of load distribution in scale-free networks. *Phys. Rev. Lett.* **87**, 278701 (2001).

670 61. Chung, F. & Lu, L. Connected components in random graphs with given expected degree sequences. *Annals Comb.* **6**, 125–145 (2002).

671 62. Cho, Y. S., Kim, J. S., Park, J., Kahng, B. & Kim, D. Percolation transitions in scale-free networks under the Achlioptas process. *Phys. Rev. Lett.* **103**, 135702 (2009).

672 63. Baird, D. & Ulanowicz, R. E. The seasonal dynamics of the Chesapeake Bay ecosystem. *Ecol. Monogr.* **59**, 329–364 (1989).

673 64. Kunegis, J. KONECT: The Koblenz network collection. In *Proceedings of the 22nd International Conference on World Wide Web*, 1343–1350 (2013).

674 65. Thompson, R. M. & Townsend, C. R. Energy availability, spatial heterogeneity and ecosystem size predict food-web structure in streams. *Oikos* **108**, 137–148 (2005).

697 **66.** Interaction Web DataBase. [http://www.ecologia.ib.usp.br/iwdb/html/thomps\\_towns.html](http://www.ecologia.ib.usp.br/iwdb/html/thomps_towns.html). Accessed: 2023-02-20.

698 **67.** Lusseau, D. *et al.* The bottlenose dolphin community of Doubtful Sound features a large proportion of long-lasting  
700 associations. *Behav. Ecol. Sociobiol.* **54**, 396–405 (2003).

## 701 Acknowledgements

702 Na.M. and K.A. acknowledge support from the Japan Science and Technology Agency (JST) Moonshot R&D (under grant  
703 no. JPMJMS2021). Na.M. acknowledges support from the National Science Foundation (under grant no. 2204936) and JSPS  
704 KAKENHI (under grant nos. JP 21H04595 and 23H03414). K.A. acknowledges support from Japan Agency for Medical  
705 Research and Development (AMED) (under grant no. JP23dm0307009), JSPS KAKENHI (under grant no. JP20H05921), and  
706 Institute of AI and Beyond at the University of Tokyo.

## 707 Author contributions

708 Na.M. conceived the research, developed the theory, performed the numerical simulations with two- and three-node networks,  
709 and drafted the manuscript. Ne.G.M. performed all the other numerical simulations. Na.M., K.A., and Ne.G.M. discussed the  
710 results, and revised and checked the manuscript.

## 711 Competing interests

712 The authors declare no competing interests.

## 713 Figure captions

714 **Figure 1.** Schematic of two networks. (a) A network with  $N = 2$  nodes connected by a directed edge. (b) A symmetric chain  
715 network with  $N = 3$  nodes. The coupling strength is denoted by  $w$ . The stress given to each node is either  $r$  or  $r - \Delta r$ .

716 **Figure 2.** An example bifurcation diagram of single-node dynamics given by Eq. (8) without dynamical noise. The solid and  
717 dashed lines represent stable and unstable equilibria, respectively.

718 **Figure 3.** Early warning signals with different node sets in a network with  $N = 2$  nodes connected by a directed edge. The  
719 solid lines represent the mean. The shaded regions represent the standard deviation. We set  $w = 0.5$ ,  $\sigma_1 = 0.1$ , and  $L = 100$ . (a)  
720 (b)  $(\sigma_2, \Delta r) = (0.1, 1)$ . (b)  $(\sigma_2, \Delta r) = (0.1, 0.5)$ . (c)  $(\sigma_2, \Delta r) = (0.2, 1)$ .

721 **Figure 4.** Early warning signals with different node sets in the undirected chain network with  $N = 3$  nodes. We set  $w = 0.05$ ,  
722  $\sigma_2 = 0.1$ , and  $L = 100$ . (a)  $\sigma_1 = 0.1$ . (b)  $\sigma_1 = 0.7$ . (c)  $\sigma_1 = 0.015$ .

723 **Figure 5.** Early warning signal,  $\hat{V}_S$ , for the maximizer of  $d$  (blue line) and a set of nodes selected uniformly at random (orange  
724 line). Both sentinel node sets are composed of  $n = 5$  nodes. We also show  $x_i^*$  for each node at each value of  $u$ . We used the  
725 coupled double-well dynamics on a BA network with  $N = 50$  nodes and gradually increased  $u$ .

726 **Figure 6.** Relationships between the Kendall's  $\tau$  and  $d$  before the first major transition in the coupled double-well dynamics  
727 on a BA network with  $N = 50$  nodes. We gradually increased  $u$ . We considered node sets  $S$  with  $n \in \{1, 2, 3, 4, 5, N\}$  nodes.  
728 (a)  $n = 1$ . (b)  $n = 2$ . (c)  $n = 3$ . (d)  $n = 4$ . (e)  $n = 5$ . (f)  $n = N$ . The  $\tau$  and  $d$  values for the node set maximizing  $d$  for each  $n$   
729 value are highlighted by the dashed lines. The cross represents “Large SD”, i.e., the node set comprised of the  $n$  nodes with the  
730 largest sample standard deviation of  $x_i(t)$ .

731 **Figure 7.** Performance of the optimized node set in anticipating the tipping point in the double-well dynamics on the BA model  
732 network with  $N = 50$  nodes. (a) Homogeneous stress and homogeneous noise. (b) Heterogeneous stress and homogeneous  
733 noise. (c) Heterogeneous stress and heterogeneous noise. The smaller symbols show the  $p_1$  and  $p_2$  values for the individual  
734 series of simulations. The larger symbols show the average over 50 series of simulations.

735 **Figure 8.** Performance of the node set maximizing  $d$  on the BA and Chesapeake Bay networks. The squares and circles  
736 represent  $p_1$  and  $p_2$ , respectively, for the given  $n$ , dynamics, network, and condition (i.e., whether  $u_i$  or  $\sigma_i$  is homogeneously or  
737 heterogeneously distributed) averaged over 50 series of simulations. (a)–(g): BA network. (h)–(n): Chesapeake Bay carbon  
738 flow network. The panels on the leftmost column correspond to the double-well dynamics, and the second to the fourth columns  
739 to the mutualistic interaction, gene regulatory, and SIS dynamics, respectively. The combination of the dynamics model and  
740 bifurcation parameter is as follows. (a) and (h): double-well,  $u$ . (b) and (i): mutualistic interaction,  $u$ . (c) and (j): gene

741 regulatory,  $u$ . (d) and (k): double-well,  $D$ . (e) and (l): mutualistic interaction,  $D$ . (f) and (m): gene regulatory,  $D$ . (g) and (n):  
742 SIS,  $\lambda$ .

743 **Figure 9.** Relationships between the Kendall's  $\tau$  and  $d$  in the coupled double-well dynamics on the BA network with  $N = 50$   
744 nodes under heterogeneous node stress and heterogeneous dynamical noise. The network is the same as the one used in Fig. 6.  
745 We considered node sets  $S$  with  $n \in \{1, 2, 3, 4, 5, N\}$  nodes. (a)  $n = 1$ . (b)  $n = 2$ . (c)  $n = 3$ . (d)  $n = 4$ . (e)  $n = 5$ . (f)  $n = N$ . The  
746  $\tau$  and  $d$  values for the node set maximizing  $d$  are highlighted by the dashed lines. The cross represents “Large SD”, i.e., the  
747 node set comprised of the  $n$  nodes with the largest sample standard deviation of  $x_i(t)$ .